



HAL
open science

Molecular-level understanding of metal ion retention in clay-rich materials

Xiandong Liu, Christophe Tournassat, Sylvain Grangeon, Andrey Kalinichev, Yoshio Takahashi, Maria Marques Fernandes

► **To cite this version:**

Xiandong Liu, Christophe Tournassat, Sylvain Grangeon, Andrey Kalinichev, Yoshio Takahashi, et al.. Molecular-level understanding of metal ion retention in clay-rich materials. *Nature Reviews Earth & Environment*, 2022, 3, pp.461-476. 10.1038/s43017-022-00301-z . insu-03714436

HAL Id: insu-03714436

<https://insu.hal.science/insu-03714436v1>

Submitted on 26 Jan 2023

HAL is a multi-disciplinary open access archive for the deposit and dissemination of scientific research documents, whether they are published or not. The documents may come from teaching and research institutions in France or abroad, or from public or private research centers.

L'archive ouverte pluridisciplinaire **HAL**, est destinée au dépôt et à la diffusion de documents scientifiques de niveau recherche, publiés ou non, émanant des établissements d'enseignement et de recherche français ou étrangers, des laboratoires publics ou privés.

Molecular-level understanding of metal ion retention in clay-rich materials

Xiandong Liu^{1†}, Christophe Tournassat^{2,3†}, Sylvain Grangeon⁴, Andrey G. Kalinichev⁵,
Yoshio Takahashi⁶, Maria Marques Fernandes⁷

1. State Key Laboratory for Mineral Deposits Research and School of Earth Sciences and Engineering,
Nanjing University, Nanjing, China

2. Institut des Sciences de la Terre d'Orléans, Université d'Orléans–CNRS–BRGM, Orléans, France

3. Earth and Environmental Sciences Area, Lawrence Berkeley National Laboratory, Berkeley, CA, USA

4. BRGM, Orléans, France

5. Laboratoire de physique subatomique et technologies associées , École nationale supérieure Mines-
Télécom Atlantique Bretagne Pays de la Loire , Nantes, France

6. Department of Earth and Planetary Science, The University of Tokyo, Tokyo, Japan

7. Laboratory for Waste Management, Paul Scherrer Institute, Villigen, Switzerland

† Corresponding author: xiandongliu@nju.edu.cn; christophe.tournassat@univ-orleans.fr.

18 Abstract

19 Clay minerals retain or adsorb metal ions in the Earth's critical zone. Rocks, sediments and
20 soils rich in clay minerals can concentrate rare earth elements (REEs) in ion-adsorption type
21 deposits and are similarly effective at metallic contaminant remediation. However, the
22 molecular-scale chemical and physical mechanisms of metal retention remain only partly
23 understood. In this Review, we describe the nature, location and energy requirements of metal
24 retention at clay mineral surfaces. Retention originates mainly from electrostatic interactions
25 during cation exchange at low pH and chemical bonding in surface complexation and
26 precipitation at neutral and high pH. Surface complexation induces surface redox reactions and
27 precipitation mechanisms including neof ormation of clay minerals layered structure. In ion-
28 adsorption type deposits, outer-sphere adsorption is the major retention mechanism of REE
29 ions. By contrast, the use of clay minerals in pollution control relies on various mechanisms
30 that can coexist, including cation exchange, surface complexation and nucleation-growth. To
31 more effectively leverage clay mineral-metal interactions in resource recovery and contaminant
32 remediation, complex mechanisms such as surface precipitation and redox reactions must be
33 better understood; for instance, by utilizing advances in quantum mechanical calculations,
34 close combination between synchrotron and simulation techniques, and upscaling of
35 molecular-level information in macroscopic thermokinetic predictive models.

36

37 [H1] Introduction

38 Clay minerals [G] play a major role in scavenging metal ions [G]¹ in Earth's critical zone [G].
39 Metal immobilization processes are key aspects of natural biogeochemical cycles in surficial
40 environments, as clay minerals can control the bioavailability of metal nutrients K⁺ and Ca²⁺
41 in temperate-zone soils². In addition, the adsorptive properties of clay-rich materials [G] make
42 them of economic interest, as they are crucial to concentrating rare earth elements (REEs) from
43 weathered granites onto clay surfaces during the formation of ion-adsorption type deposits³.
44 Clay-rich materials are also of growing industrial interest owing to their effective metal
45 retention capacity and their cheap, widespread availability. For example, clay minerals are
46 commonly used in pollution control and remediation applications, including as containment
47 barriers in radioactive waste repository concepts⁴, as liner materials in landfills⁵, or as
48 remediation agents for heavy metal-polluted soils⁶. The interaction of clay minerals and metal
49 ions is therefore critical to environmental, industrial and economic applications. However, the
50 complex and diverse nature of clay minerals and their surfaces mean that the mechanisms of
51 metal retention remain debated.

52 The distinctive interaction of clay minerals with metal ions stems from their surface properties,
53 which result from their layered crystal structure (Box 1 and Figure 1)⁷. Individual clay layers
54 are formed of an octahedral sheet [G] sandwiched between two tetrahedral sheets [G], often

55 called **2:1 layers [G]** (Figure 1). When stacked together, these layers create inner, outer and
56 edge surfaces onto which metal ions can be adsorbed. However, each layer can have varying
57 compositions, meaning OH groups and cation exchange sites have a range of surface positions
58 (Box 1). Various OH groups exist (such as those coordinated to Si, Al, Mg, Fe) and they are
59 responsible for the chemical bonding of metal ions. This variety of surface positions, surface
60 groups and layer compositions lead to a diversity of retention processes, such as cation
61 exchange, surface complexation, structural incorporation in clay layers or through mineral
62 growth by **epitaxial nucleation [G]**⁸.

63 Bulk measurements of metal retention in batch experiments do not always provide enough
64 information to predict the fate of metal ions in practical or real-life applications in clay-rich
65 media. Extrapolating the results of batch adsorption experiments (with timescales from hours
66 to days) directly to radionuclide retention predictions in radioactive waste disposal in a
67 geological formation (with timescales over hundreds and thousands of years) can lead to
68 erroneous conclusions because the various retention processes do not have the same kinetic
69 and reversibility characteristics. Consequently, molecular-level knowledge is crucial for
70 understanding the physical-chemical mechanisms underlying experimental and field
71 observations, and for developing predictive models for these environments^{6,9}.

72 The emergence of several experimental techniques (such as **neutron diffraction¹⁰ [G]**,
73 **synchrotron X-ray reflectivity (XRR)¹¹ [G]** and **X-ray absorption spectroscopy (XAS) [G]^{12,13}**)
74 in the late 1980s, accompanied by the rapid development of computational modelling
75 approaches (quantum mechanical, classical and multiscale)¹⁴, has provided the necessary tools
76 for exploring clay mineral-metal ion interactions over different time scales. Because of the high
77 surface heterogeneity of clay minerals, some of the basic properties controlling metal ion
78 retention can be quantified only with the combination of advanced experimental and molecular
79 simulation methods. Multiscale simulation methods in particular are a powerful tool for
80 providing parameters that are impossible or very difficult for experiments to achieve, such as
81 predicting the behavior of metal ions in clay-rich media over geological timescales¹⁵.

82 In this Review, we discuss advances in understanding metal ion-clay mineral interactions at
83 the molecular scale. We first explore the macroscopic factors that affect the adsorptive
84 properties of clay minerals, such as the composition and pH of the aqueous solution. Next,
85 immobilization processes are described separately for basal and edge surfaces because they
86 have fundamental differences in bonding mechanisms of with metal ions. We then review the
87 importance of metal retention processes in ion adsorption REE ore formation and pollution
88 control engineering, and we highlight possible future research directions in the molecular-level
89 view of clay mineral-metal ion interactions for fundamental and applied research.

90

91 [H1] Macroscopic environmental factors

92 Under favourable conditions, 1 kg of smectite [G] such as montmorillonite can sorb up to 100
93 g of metal cations, or equivalently about 1 mol of a monovalent metal cation. This capacity
94 depends, of course, on local environmental conditions. Factors most impacting adsorption
95 processes on clay mineral surfaces are pH and ionic strength. Depending on the chemical
96 properties of the metal ions of interest, either one or both of these parameters can influence its
97 overall retention (Box 2). For example, adsorption of alkaline and alkaline-earth metal ions in
98 their cationic form such as rubidium (Rb^+)^{ref 16–19}, cesium (Cs^+)^{ref 20,21}, strontium (Sr^{2+})^{ref 22,23},
99 and barium (Ba^{2+})^{ref 19} is little impacted by pH, and strongly depends on ionic strength, while
100 adsorption of more easily hydrolysed transition metals such as nickel (Ni^{2+})^{ref 24,25} and cobalt
101 (Co^{2+})^{ref 26–28}, REEs, such as europium (Eu^{3+})^{ref 26,29}, and actinides^{ref 30}, such as uranium (UO_2^{2+})
102^{ref 29}, is affected by both parameters. Because adsorption can be a competitive process at surface
103 sites, the chemical composition of the aqueous solution is also an important factor that
104 contributes to the effectiveness of retention^{31–33}. Also, the presence of dissolved and adsorbed
105 organic molecules can be beneficial or detrimental to metal ions adsorption on clay mineral
106 surfaces^{22,34}.

107 Macroscopic quantification of cations retention on smectite and illite [G] surfaces amounts for
108 countless studies in the literature (see references in³⁵) whereas studies concerning the retention
109 of anionic species are more limited. Repulsive electrostatic interactions are responsible for
110 anions repelling from the surface, and thus many anionic element do not sorb substantially on
111 illite and montmorillonite surfaces, such as iodide (I^-), pertechnetate (TcO_4^-), and selenate
112 (SeO_4^{2-})^{ref 36,37}. Some anions, including metalloids, sorb weakly, but notably, such as selenite
113 (SeO_3^{2-})^{ref 36,38–41}, arsenate (AsO_4^{3-})^{ref 42–45}, arsenite (AsO_3^{3-}), antimony (in the forms $\text{Sb}(\text{OH})_3$
114 or $\text{Sb}(\text{OH})_6^-$)^{ref 46}, and molybdate (MoO_4^{2-})^{ref 47}. Adsorption dependences on environmental
115 parameters are also different, often opposite, for anions compared to cations. For example,
116 SeO_3^{2-} adsorption decreases with increasing pH, but is independent of ionic strength. For
117 AsO_4^{3-} , adsorption on illite and montmorillonite increases up to pH 5-6 and then decreases at
118 higher pH. Because adsorption of anions is much less efficient than of cations, clay materials
119 are not often studied as promising materials for applications relying on anion retention
120 properties such as pollution control engineering. This statement must be however reconsidered
121 if modifications of clay mineral surface properties are obtained through interactions with
122 organic molecules. So-called organo-clay materials have proven to be very effective in
123 removing oxyanions such as hexavalent chromium (CrO_4^{2-})^{ref 48}. This Review is focused on
124 interactions of metal ions with unmodified clay materials. Consequently, it is also mostly
125 focused on interactions with metal cations.

126 The reasons for these differences among cations, as well as between cations and anions, were
127 early ascribed to differences in interaction mechanisms on basal and edge surfaces with two
128 main mechanisms⁴⁹ (Figure 2). The first one is **inner-sphere complex [G]** reactions, in which
129 metal ions compete with protons (H^+) for the adsorption sites on edge surfaces, and the second
130 is cation exchange reaction, in which metal ions replace layer charge compensating cations on

131 basal surfaces through, mostly, **outer-sphere complexes [G]**. Anions can also bind through
132 ligand exchange [G] to form inner-sphere complex and in that case anions compete with edge
133 hydroxyl and water surface groups. Because of the non-linearity of cation adsorption isotherms,
134 it was soon necessary to subdivide edge surface complexation sites into two categories, the so-
135 called strong and weak sites⁵⁰, which made it possible to account for the higher affinity of some
136 metal ions for the surface at low equilibrium concentration. Competitive adsorption
137 experiments³³ evidenced the need to define sub-categories of strong sites, meaning sites that
138 are least abundant but most energetically favourable to retention, for which some metal ions
139 do compete and some others do not.

140 Macroscopic observations of metal ion retention on clay mineral surfaces can be understood in
141 principle by considering two main types of surface complexes on basal and edge surfaces. The
142 rationale behind most of these macroscopic modelling concepts remains very empirical, but
143 can be verified by progresses made in the molecular level view of the adsorption processes.

144 **[H1] Molecular-level interaction mechanisms**

145 Multiscale experimental and modeling approaches rooted in molecular level information (Box
146 3) are necessary to unravel the relative contributions of both the diverse array of metal ion
147 retention mechanisms and the associated reactive sites on clay surfaces. Basal surfaces are
148 terminated by saturated oxygen atoms whereas edge surfaces exhibit broken chemical bonds,
149 leading thus in differences in reactivity between these two types of surfaces and metal ions.
150 Hence, these interactions are discussed separately, and the influence of environmental
151 parameters such as hydration state and the presence of organic matter are then introduced.

152 **[H2] Basal surfaces**

153 At basal surfaces, metal ions cannot form easily covalent bonding with surface atoms, which
154 are already fully coordinated. Species adsorbed at basal surfaces are thus bound through weak
155 long-range interactions such as electrostatics, which are the most effective for cations
156 interacting with the negative potential created by the permanent negative charge of the layer.
157 The adsorption state of cations largely depends on the Gibbs free energy of dehydration, that
158 is, the cost in free energy of partial dehydration (such as, losing water ligand to form direct
159 contact with the surface) makes the formation of inner-sphere complexes unfavourable.
160 Therefore, most cations such as Li^+ , Na^+ and those of higher valences form outer-sphere
161 complexes while K^+ , Rb^+ and Cs^+ form inner-sphere complexes due to lower dehydration free
162 energy. The inner-sphere complexing sites include the positions above the center of ditrigonal
163 cavity and above tetrahedron⁵¹⁻⁵³. Adsorbed cations compete with other cations present in
164 solution, hence the dependence of adsorption on ionic strength and on background electrolyte
165 composition⁵⁴.

166 The cation exchange thermodynamic theory makes it possible to conduct predictive
167 quantifications without the need for molecular level understanding^{55,56}. It has however several

168 drawbacks including the difficulty to derive true thermodynamic equilibrium constants and
169 activity coefficient of exchanged species⁵⁷. This problem often leaves exchange model
170 parameters to the status of conditional constants that should not be applied without caution to
171 conditions too different from the corresponding experimental conditions⁵⁸.

172 Cation exchange models can be enriched with the consideration of multiple sites present on a
173 same clay mineral particle, and having contrasting affinities for metal ions adsorption. Cs⁺
174 exchange on illite surfaces represent certainly the best example for this need of a multiple sites
175 description^{20,59,60}. Cs⁺ affinity for illite surface decreases by several order of magnitude with
176 the increase of aqueous Cs⁺ equilibrium concentration. The presence of at least three types of
177 exchange sites is necessary to explain this behaviour. The least abundant site must have also
178 the highest affinity for Cs⁺ and is ascribed to the presence of so-called frayed edge sites⁶⁰,
179 which correspond to adsorption sites on basal surfaces neighbouring the edge of illite particles⁶¹.
180 The two other sites have been ascribed to illite basal surfaces as the sum of their capacities
181 matches illite cation exchange capacity, but the reason for their contrasted affinities for Cs⁺
182 remains unclear⁶⁰. This example illustrates the underlying complexity of adsorption processes
183 on basal surfaces.

184 Quantitative techniques in numerical simulation are now available to evaluate the profiles of
185 cation adsorption free energy as functions of their distance from the basal clay mineral
186 surfaces⁶², and these techniques can take into account the effects of layer charge distribution
187 on these surfaces and distinguish between several specific adsorption sites⁵¹. Molecular
188 simulations coupled to X-ray reflectivity and resonant anomalous X-ray reflectivity
189 measurements provided evidence of the importance of interfacial water structure on the affinity
190 of cations such as Rb⁺ and Cs⁺ for outer basal surfaces of phyllosilicates^{51,63,64}. Differences in
191 the structure of water in the hydration shell lead to multiple adsorption positions for a single
192 cation at a single surface, which could be a reason for the observed changes in macroscopic
193 affinities as a function of cation concentration^{59,65–67}.

194 In interlayer domains of **swelling [G]** clay minerals, cations and their hydration sphere interact
195 with both bordering inner basal surfaces⁶⁸. The layer-to-layer distance depends on the hydration
196 of interlayer cations and on the external pressure applied to the clay-rich material⁶⁹. Conversely,
197 experimental values of montmorillonite interlayer affinity for Cs⁺ increase with the pressure
198 applied to the system, and hence with the change of interlayer occupancy from three water
199 layers to two and one water layer(s)⁷⁰. According to molecular dynamics simulations and
200 microcalorimetric experiments, the main driving force for Cs⁺ adsorption on clay mineral
201 surface is not the a priori energetically favourable Cs⁺-clay mineral interaction, but the relative
202 hydrophobicity of Cs⁺ compared to its cationic competitors for the surface^{51,52,64,71,72}. This
203 molecular level information should help to build advanced cation exchange models that
204 consider several energy terms to describe properly metal ions adsorption as a function of usual
205 parameters such as concentrations, but also as a function of temperature, pressure and related
206 hydration state encountered in underground clay-rich geological settings.

207 Most of the classical atomistic simulations of hydrated cation interactions with basal clay
208 mineral surfaces only include the effects of molecular and ionic polarizability in an implicit

209 way through the effective parameters of interatomic interactions⁷³. However, more advanced
210 models explicitly including the polarizability effects into calculations are also emerging^{74,75}.

211 Beyond the possibility to better describe and quantify metal ions affinity for basal surfaces,
212 simulations and experiments at the molecular level offer a unique capability to study the
213 mobility of surface species as a function of their location. The standard view of adsorbed
214 surface species immobilized in the Stern layer is contradicted by evidences from molecular
215 dynamics simulations⁷⁶⁻⁷⁹ and spectrometric measurements, such as nuclear magnetic
216 resonance⁷⁹, which show substantial in-plane diffusion of species adsorbed on basal surfaces.
217 Growing macroscopic experimental evidences about this coupling is also made available and
218 macroscopic modelling of diffusive transport of metal ions in clay-rich materials has evolved
219 accordingly since the early ~2010s' to take these coupled adsorption/diffusion processes fully
220 into account^{14,80-82}, with important implications for the modelling of the performance of
221 radioactive waste storage concepts in clay-rich geological formations⁸³⁻⁸⁵. Because of the
222 highly coupled nature of these processes, molecular level information is necessary to decipher
223 the relative contributions of the various types of adsorbed species in interlayer, Stern layer and
224 in the diffuse layer⁸⁶.

225 Because of the chemistry and structure of clay mineral layers, electrostatics is the dominating
226 interaction at basal surface, making the formation of outer-sphere complex the major metal
227 retention mechanism, except for cations having low dehydration free energy, which can be
228 adsorbed as inner-sphere complexes. This apparent simplicity of interaction mechanism
229 description is however hiding additional complexity arising from coupling with environmental
230 parameters, such as pressure, or with other physical processes such as ion mobility.

231 **[H2] Edge surfaces**

232 Higher chemical reactivity leads to the higher diversity of interaction processes on edge
233 surfaces. Surface complexation first occurs when edge groups gradually become available for
234 complexing cations upon proton dissociation as pH increases. Further accumulation at higher
235 pH can cause surface nucleation and crystal growth. In the meanwhile, interfacial electron
236 transfer processes can participate in the interactions of redox-active metal ions with Fe-
237 containing clay minerals.

238 **[H3] Surface complexation**

239 Clay minerals edge surface structure is responsible for a wide range of possible adsorption sites
240 and processes, with adsorbates having the possibility to interact by surface complexation or
241 ligand exchange with tetrahedral sites, octahedral sites or both, and by different binding modes
242 such as mono- or multi-dentate surface complexes. Depending on the chemical nature of these
243 sites (for example Al octahedra versus Mg or Fe octahedra), binding affinities with adsorbates
244 can also vary. In addition, site coordination depends on the crystallographic plane of each edge,
245 which adds up this complexity⁸⁷⁻⁸⁹. The corresponding diversity of site types provides a
246 reasonable explanation to the necessity to consider many sub-categories of edge adsorption

247 sites in surface complexation models. However, it highlights also the necessity to better
248 constrain the nature of the surface complexation sites to understand competition processes.

249 Spectrometric techniques, such as X-ray absorption fine structure (EXAFS) spectroscopy, and
250 diffractometric techniques, such as high-energy diffractometric methods, and more specifically
251 differential X-ray pair distribution function (d-PDF), provide molecular level information to
252 unravel retention processes on clay mineral edges. For example, d-PDF measurements
253 evidenced the binding mode of Sb(V) on montmorillonite to be a bidentate complex attached
254 to the edges of the octahedral sheet⁹⁰. While d-PDF can be used to decipher the crystallographic
255 nature of surface complexation adsorption sites on clay minerals, some limitations of the
256 technique prevent its general use in adsorption studies. These limitations include the needs of
257 a high adsorbed concentration of the element of interest, and an a priori knowledge of the
258 structure of clay mineral edges, which must remain unaffected during the experiment. Such
259 limitations are partly circumvented by the use of EXAFS spectroscopy that allows determining
260 and quantifying the local environment of adsorbed elements.

261 In experimental conditions identified as being favourable to surface complexation on strong
262 sites Ni²⁺ adsorbs only in octahedral coordination in plane with the octahedral sheet on
263 montmorillonite edges⁹¹. Adsorbed Zn exhibit a similar local environmental on
264 montmorillonite strong edge sites. In conditions favourable to adsorption on weak sites, Zn had
265 a more disordered configuration, possibly related to the presence of multiple adsorption sites,
266 all being out of the clay mineral octahedral plane⁹² and possibly being bidentate complexes⁹³.
267 For the adsorption of lanthanides, such as Eu, on illite and montmorillonite edge surfaces.
268 Time-resolved laser fluorescence and EXAFS spectroscopy indicate the formation of inner-
269 sphere surface complexes at pH >5 for both clay minerals^{29,94,95, 192-194}. Correspondingly,
270 surface complexation of Eu, other lanthanides and trivalent actinides on illite and
271 montmorillonite can be modelled successfully with the same surface complexation model
272 approach as that used for transition metals^{27,29,96}.

273 While diffractometric and spectrometric methods give insightful details about adsorption
274 processes, they are often limited by the presence of multiple surface complexes that cannot be
275 probed individually, and by the impossibility to distinguish a site configuration from another
276 because of a lack of sensitivity of the method. This limitation can be overcome by coupling
277 molecular level simulation predictions with diffractometric/spectrometric information. For
278 example, the combination of FPMD simulations with EXAFS spectroscopy results made it
279 possible to assign the outermost **dioctahedral [G]** vacancy of dioctahedral layers to strong sites
280 for Zn²⁺ and 1st row transition metals^{93,97,98}, while other sites are related to weak sites, such as
281 aluminol, silanol, apical oxygen and their combination⁹⁷ (see principle in Figure 3). Another
282 interesting example is the complexation of uranyl on montmorillonite surfaces, for which
283 different macroscopic modelling approaches yielded different interpretations about the binding
284 mode and the sites available for this species^{99,100}, while being equally good at predicting
285 available macroscopic retention observations as well as spectroscopic results. A possible
286 physical basis was later provided by molecular level simulations. While multiple bidentate
287 complexes were predicted by static density functional theory (DFT) calculations¹⁰¹⁻¹⁰³, first

288 principles molecular dynamics (FPMD) simulations showed that they have similar binding
289 affinity and therefore can be treated with a single stability constant in a macroscopic surface
290 complexation model¹⁰⁴. This example highlights that the determination of adsorption sites in
291 case of surface complexation, both from microscopic and macroscopic points of view, is an
292 extremely complex task, which requires the coupled use of several experimental and
293 computational physical and chemical methods to obtain reliable results (Figure 3).

294 This identification of surface adsorption sites is made even more complicated in systems
295 resembling to natural conditions with the possible interactions of aqueous components and
296 surfaces in ternary (or more) surface complexes. The uranium-carbonate-montmorillonite case
297 is very informative in this respect. This system has been investigated using EXAFS
298 spectroscopy by several teams, yielding different interpretations of uranium binding
299 mechanisms^{100,105,106}, with the reported presence¹⁰⁵ or absence¹⁰⁰ of ternary uranyl-carbonate-
300 montmorillonite complexes for experiments conducted in similar conditions. Additional
301 constraints provided by molecular level simulations of ternary complexes adsorption processes
302 would certainly help to resolve this apparent inconsistency.

303 [H3] Nucleation and growth

304 At high pH values and in the presence of high concentrations of metal ions, surface complexes
305 can serve as nucleation sites, thus promoting (co-)precipitation of metal ions. Epitaxial
306 nucleation or growth has been found for the 1st row transition metal including Zn²⁺ ref 107,108,
307 Ni²⁺ ref 109,110, Co²⁺ ref 111 and Fe²⁺ ref 112,113. The neoformed phases can be a phyllosilicate or a
308 layered double hydroxide (LDH). LDH, similar to hydroxalcite, is made up of stacked
309 octahedral layers, where the partial substitution of trivalent for divalent cations results in a
310 positive layer charge, compensated by anions located in interlayer space. Because of structural
311 similarities between the neoformed octahedral layer and the octahedral sheet of TOT layer, it
312 is reasonable to assume that these phases nucleate and grow as a continuation of the edges
313 (Figure 2). FPMD simulations¹¹⁴ evidenced that upon complexation in vacancy, these elements
314 hydrolyse in normal pH range and thus provide complexing sites for subsequent metal cations,
315 eventually yielding epitaxial nucleation. In contrast, cations with larger ionic radii like Pb²⁺
316 hardly hydrolyse on clay mineral surfaces, prohibiting the multinuclear complexation and
317 nucleation. Phyllosilicates would form in presence of considerable amount of Si in solution, in
318 laboratory as well as in natural systems^{12,108,115-117}. In samples from Zn-clay ores, transmission
319 electron microscopy evidence was found for epitaxial growth of Zn-smectite from clay mineral
320 edges which played a templating role¹¹⁸. FPMD study suggested that for the formation of
321 phyllosilicates, the synchronous pathway (that is Si and metal ions co-precipitate at the same
322 time, path G to H in Figure 2) is favourable over the stepwise pathway (that is the phyllosilicate
323 is formed via silicification of neoformed hydroxide, path I to J in Figure 2)¹¹⁴.

324 Actinides and lanthanides can also form secondary mineral phases⁹⁴. Because of obviously
325 larger ionic radii of f-elements, actinides and lanthanides cannot form phyllosilicate/hydroxide
326 phase resembling the structure of clay minerals. In these cases, clay minerals might only
327 provide complexing ligands, for example, in the formation of coffinite (U(IV)SiO₄), but have

328 no templating effect. Although classified as REEs together with lanthanides and Y, Sc can be
329 incorporated into octahedral sheets, forming Sc-rich smectite¹¹⁹.

330 [H3] Surface redox reactions

331 Clay minerals often contain structural or adsorbed Fe^{ref 120}, which participate in electron
332 transfer reaction with adsorbed redox sensitive metal ions¹²¹, such as U^{ref 122–124}, Np^{ref 124}, Pu
333 ^{ref 125,126}, Se^{ref 127,128}, Tc^{ref 124,129–131}, and Cr^{ref 131–135}. The mobility of redox sensitive elements
334 depends on their oxidation state, often through the contrasted solubility and adsorption
335 properties of oxidized and reduced aqueous species of a given element. The study of surface
336 enhanced reduction or oxidation of redox sensitive metal ions is made very difficult by the
337 numerous mechanisms that were identified as a function of the elements of interest, but also as
338 a function of the nature of the clay mineral and of the geochemical conditions. For example,
339 naturally reduced ferrous clay minerals from subsurface redox transition zones exhibit
340 minimal reactivity towards the oxyanions TcO₄⁻ and CrO₄²⁻ compared to those measured in
341 previous studies on laboratory treated samples¹³¹. Their reduction capacity was enhanced by
342 adsorbed Fe(II) although added Fe(II) was not detected as redox-reactive species within the
343 outermost few nanometers of clay mineral surfaces. The adsorption of Se(IV) on
344 montmorillonite is an another example of a surface-enhanced redox reaction. In the presence
345 of dissolved Fe(II) and in the pH range (pH < 8) where Fe(II) is also sorbed onto
346 montmorillonite, a reductive precipitation of Se(IV) to nano-particulate Se(0) in the pH range
347 (pH < 8) is observed^{127,136}. However, based on Mössbauer spectrometry and XANES
348 measurements, Fe oxidation kinetic rate was much higher than Se reduction kinetic rate.
349 Structural Fe(II) in a chemically reduced nontronite does not reduce As(V) or Sb(V), and when
350 all structural Fe is Fe(III), it does not oxidize As(III) and Sb(III) neither. Also, Fe(III) within a
351 Fe(II)–O–Fe(III) moiety is more reactive compared to that in Fe(III)–O–Fe(III) in oxidizing
352 As(III) and Sb(III)^{ref 128,137}, and so, Fe(II)–O–Fe(III) moieties at the edge sites are assumed to
353 be the redox-active species in Fe-containing clay minerals.

354 Electron transfer processes at mineral interfaces can in principles be modeled by using DFT
355 based free energy calculation methods^{138,139}. However, the delocalization error caused by the
356 poor description of the exchange energy in generalized gradient approximation (the commonly
357 currently used DFT level) usually leads to errors in the estimates of redox levels and redox
358 potentials, with the underestimate in redox potential reaching 1 eV¹⁴⁰. The estimate of redox
359 levels and redox potentials could be improved to some extent by using the *beyond DFT*
360 *technique*, such as Hubbard+U¹⁴¹ and constrained DFT¹⁴². These techniques have also been
361 used to estimate the rate of self-exchange type electron transfer¹⁴³. However, such ad hoc tricks
362 can bring about other problems. Advanced functionals such as hybrid/double-hybrid functional
363 are able to obviously improve the predictions, for aqueous transition metal cations¹⁴⁴, liquid
364 water¹⁴⁵ and solid-water interfaces¹⁴⁶. Unfortunately, FPMD using these functionals are easily
365 tens of times more expensive than that with generalized gradient approximation. The
366 computational cost has now been a major obstacle to the application on the mineral interfaces
367 of geochemical/environmental interest. Understanding the redox properties and the associated
368 electron transfer mechanisms in clay minerals is thus a key but also challenging issue on an
369 experimental as well as from a computational point of view.

370 [H2] Influence of environmental parameters

371 [H3] Water saturation and surface hydration

372 Clay mineral surfaces are hydrated in conditions relevant to the critical zone. Water molecules
373 are adsorbed through interactions with both adsorbed cations and clay surface atoms. A 43 %
374 relative humidity is sufficient for external basal surface to be covered by a complete water layer,
375 which corresponds to dry conditions in Earth's surficial environments. Relative humidity of
376 only 0.2 % and 9 % are sufficient to establish fully hydrated smectite interlayer space with
377 monolayer and double layer states respectively^{147,148} because of strong water attraction under
378 nanosized confinement. Previous simulation and experimental studies indicate that under
379 partially saturated conditions, outer-sphere complexes can transform into inner-sphere, that is,
380 the adsorption is stronger compared to water saturated condition^{76,149}. On the opposite,
381 adsorption of Cs⁺ on the outer-basal of montmorillonite decreases with decreasing water
382 saturation levels in adjacent interlayer spaces⁶⁷, thus evidencing also possible long-range
383 interactions influencing cation adsorption from one surface to another surface in clay mineral
384 particles. This effect seems, however, to have a minor influence on cation mobility in clay-rich
385 materials compared to the effect of pore connectivity decrease with decreasing water saturation
386 levels¹⁵⁰.

387 [H3] Natural organic matter

388 In soil and sedimentary rock systems, the presence of organic matter brings in additional
389 complexity on retention of metal elements¹⁵¹. Natural organic matter and clay minerals form
390 organo-clay association through the bonding of active groups, such as carboxylate, phosphate,
391 and ammonium groups, and hydrophobic interactions with aliphatic or aromatic moieties¹⁵².
392 Organic matters can bind on outer basal and edge surfaces and can also intercalate into the
393 interlayer region of clay minerals¹⁵³, with binding location and mechanism varying as a
394 function of factors such as pH, ionic strength¹⁵².

395 Because of the multifunctionality of natural organic matter, they can alter surface
396 hydrophilicity, cover surface sites while they bring in active groups which can serve as
397 complexing sites for metal cations, and they can take part in interfacial electron transfer
398 processes with redox-active groups¹⁵⁴. Consequently, the effect of organic matters on metal
399 cation retention in clay-rich materials can be extremely complicated, and the presence of
400 organics can promote or inhibit the retention of metal ions depending on investigated metals
401 and experimental conditions^{22,34}.

402 The molecular-level mechanisms that are responsible for organic matter – metal ions – clay
403 minerals interactions are still far from being fully understood. Natural organic matter are now
404 described as supramolecular associations of a group of small molecules^{155,156} rather than
405 macromolecules¹⁵⁷ or polymers¹⁵⁸, as evidenced by both experiments^{159,160} and molecular
406 simulations¹⁶¹. By taking advantage of this new description of organic matter structure,
407 molecular level models of organo-clay associations have been developed, which can explicitly
408 take account of experimentally measured properties of organics and clay minerals^{162,163}. Such
409 models together with multiscale simulation techniques can thus serve as a starting point to

410 explore microscopic interactions and develop predictive approaches for multicomponent
411 systems.

412 Clay mineral edge surface reactivity is responsible for very diverse interaction processes with
413 metal cations, including surface complexation, co-precipitation and redox reactions, which
414 cannot be unravelled on the basis of batch chemical characterization only. Because the kinetics,
415 reversibility, and thus efficiency of these retention processes are not the same depending on
416 environmental conditions, deciphering their respective contributions is necessary to make
417 useful predictions for industrial and environmental applications. Multiscale experimental and
418 modeling approaches rooted in molecular level information have proved to be effective to do
419 so (Figure 3), but many technical challenges remain, especially to model crystal growth and
420 redox reactivity.

421 **[H1] Industrial and environmental implications**

422 Major advances in the ability to characterize and model interaction processes and mechanisms
423 have important practical applications to several environmental and industrial processes. Below
424 we briefly describe the current understanding of clay mineral-metal ion retention processes in
425 both metallic waste pollution control and REE ion-adsorption deposits as examples.

426 **[H2] Pollution control engineering**

427 Clay minerals have exceptional thermal, mechanical, hydraulic and chemical properties, they
428 are abundant in nature and reasonably cheap. Because of these features, clay-rich materials are
429 commonly used as natural buffers to remediate contaminated soils and waters and to inhibit the
430 migration of pollutants in disposal facilities for hazardous wastes including radioactive
431 waste^{9,164–169}. Clay minerals are also increasingly finding new applications in materials science,
432 biotechnology and clay mineral-based nanocomposites development^{166,170}.

433 Adsorption is one of the most efficient mechanisms to remove metal ions, which is why clay
434 minerals have been used since the ~1970-1980s as a less toxic alternative for environmental
435 remediation. However, in the face of increasing pollution from industrial and anthropogenic
436 activities, increasing efforts have been made since the ~2000s to develop new types of clay
437 mineral-based adsorbents modification of natural clay-rich material to increase its adsorption
438 capacity, such as modified clay minerals and nanocomposites. Clay mineral-based adsorbents
439 are used for the removal of toxic organic and inorganic (metal) contaminants from polluted
440 waters. The removal efficiency of clay minerals towards pollutants can be increased through
441 treatments of the material such as thermal and acid treatment, exfoliation, pillaring of cations,
442 and modification with surfactants, polymers and organosilanes^{171–173}.

443 Clay mineral supported nanoparticle have high potential for use in the development of high-
444 capacity adsorbents and photocatalyst. Montmorillonite supported zero-valent iron is very
445 effective in removing highly toxic arsenic from aqueous solutions¹⁷⁴. The combination of many
446 type of modification and the use of clay minerals of various morphologies (tubed, fibrous,

447 stacked) has led to the development to tailored made clay mineral based nanomaterial(s) with
448 extreme high and selective adsorption properties^{175–177}. For instance, polymer-functionalized
449 clay mineral nanocomposites combine the remarkable features of both nanoparticles and
450 polymers. The use of clay mineral as a nanofillers in polymer matrixes confer the polymer
451 desirable interfacial properties^{178,179}.

452 Most studies published in the field of pollution control engineering focus on aqueous
453 contaminant removal efficiency of raw and treated clay-rich materials, and on the associated
454 favorable environmental or engineered conditions. In proportion of the total number of studies,
455 few gain insights from basic molecular understanding about retention processes. Notable
456 exceptions to this dominant empiricism driven approach are found in the areas of radioactive
457 waste storage^{9,180}, and of the study of mobility of metals in soils^{59,181,182}, for which cation
458 exchange, surface complexation, surface precipitations, electron transfer, as well as
459 interactions with natural organic matters have been identified as important clay mineral related
460 processes in the understanding of metals mobility and biogeochemical cycling.

461 Geological disposal, which is presently the internationally preferred option for the storage of
462 radioactive waste, relies on a multi-barrier concept, which is a combination of engineered
463 barriers (waste form and canister, backfill, seal) and natural barriers (host rock), to ensure the
464 containment and long-term isolation of the highly radio- and chemo- toxic waste from the
465 biosphere. Clay minerals are key components of such most multi-barrier systems. The retention
466 of (radio-)contaminants on clay minerals surfaces along potential transport paths is the main
467 retardation mechanisms on which the safety assessment of deep geological repositories relies
468 (Figure 3).

469 Because of the time- and length scales envisioned for radioactive waste storage, the prediction
470 of contaminant migration in performance and safety assessments are commonly based on
471 models using a limited set of macroscopic parameters, on which sensitivity analysis are
472 conducted. These macroscopic parameters loop together many basic processes (Figure 3). For
473 example, all retention mechanisms explored in this review are often up-scaled in the form of a
474 single numerical parameter for a given radionuclide. In this respect, the safety case must
475 demonstrate a detailed understanding of the physical–chemical phenomena governing retention
476 processes, in order to confirm the consistency of the chosen up-scaling approach⁹ (Figure 3).

477 Retardation factors (R_f), which quantify the delayed aqueous transport of adsorbed
478 contaminants compared to a perfect tracer, are major input parameters in performance and
479 safety assessments⁸³. R_f values for strongly adsorbing tracers are commonly derived from K_D
480 values measured from batch adsorption experiments. Since the ~2000s, evidence of coupled
481 transport-retention processes through surface-enhanced diffusion have accumulated, which
482 questions the adequacy of this equivalence between real R_f values and R_f values derived from
483 batch K_D values. Related experimental and modelling study at all scales from molecular
484 level^{15,81} to in situ tests^{183–185} gave rise to changes in modelling paradigms with consideration
485 of emergent coupled processes^{82,83}, in which part of adsorbed species is not immobilized on
486 the surface, but, on the contrary, participates to an enhancement of the overall diffusion flux<sup>186–
487 188</sup>. Adsorption must be seen as a process that both slows down metal ion transfer because of

488 accumulation on the surface, and also that accelerates their transfer through surface-enhanced
489 diffusion. Consequently, a detailed understanding of adsorption process must be made
490 available to use retention parameters obtained in static systems for the prediction of
491 contaminants diffusive mobility.

492 [H2] Ion-adsorption REE ores

493 REEs ion-adsorption type deposits (IADs) have been known as an important source of REEs
494 in the world in particular for heavy REEs^{189–194}. IADs are characterised by high recovery rate
495 of REEs simply by leaching of REEs with an ammonium sulphate solution at normal
496 temperature, and low leachable amounts of U and Th, which can cause problems in other REEs
497 sources in terms of environmental problems and working environment. Thus, IADs are ideal
498 REE resources, which are critical to society due to its use in modern technologies^{195,196}.

499 IADs are mainly found in weathered profile of felsic igneous rocks with a variety of clay
500 minerals. In most cases, weathered granite has been developed, but IADs can also be found in
501 felsic volcanic rocks in the world^{191,193,197–199}. IADs typically consist of a strongly weathered
502 zone at the surface layer, and an enriched zone of REEs in the subsurface layer accumulated
503 mainly by adsorption through outer-sphere complexation of hydrated REE trivalent cation to
504 clay minerals (Figure 4a,b)^{189,199,200}. The surface layer exhibits a positive Ce anomaly in REE
505 patterns due to the removal of the other REEs and fixation of Ce by its oxidation to insoluble
506 Ce(IV) species^{201,202}, whereas the subsurface REE-enriched layer generally shows a negative
507 Ce anomaly due to the fixation of REEs, except for Ce (Figure 4c-e).

508 REE species in the enriched zone have been revealed by EXAFS spectroscopy^{189,200}, showing
509 that the outer-sphere surface complex to clay minerals is main REE species, and the species is
510 responsible for the high recovery rate of REE by the ion-exchange reaction^{192,203}. These results
511 are consistent with laboratory studies on the formation of outer-sphere complex to various clay
512 minerals, such as montmorillonite, as evidenced by EXAFS spectroscopy^{189,200,204} and by laser-
513 induced fluorescence spectroscopy^{205,206}. The enriched zones are usually located in acidic
514 environment ($\text{pH} < 6$)¹³⁸. The lower pH is unfavorable for dissociation of groups of edge
515 surfaces, thus suppressing the formation of REE inner-sphere complexes. Although the
516 identification of phyllosilicates at the nm-scale is possible by transmission electron microscopy,
517 the detection of REEs in the same view presented a challenge, which inhibited the attainment
518 of clear identification of the REE host phase. In such cases, secondary ion mass spectrometry
519 (SIMS) can bring additional insights²⁰⁷. Identification of the host mineral is primarily important,
520 since the type of host mineral is related to the degree of weathering depending on temperature
521 and rainfall²⁰⁸, which is crucial information for the survey of IADs, and the recovery rate of
522 REE from the IADs.

523 High REEs extractable property of IADs is very contrastive to marine REEs resources such as
524 marine ferromanganese oxides with low extractability of REEs ($< 1\%$) due to the formation of
525 inner-sphere surface complex of REEs^{209–212} and deep-sea REEs-rich mud with REEs
526 incorporated as phosphate phases²¹³. However, IADs cannot be formed under marine
527 environment due to high salinity of seawater, which shows that IADs are specific to land areas.

528 The difference between IADs and marine ferromanganese oxides originated from the different
529 REE retention mechanisms: the former is mainly through electrostatics which is hindered by
530 high ionic strength, whereas the latter is through chemical bonding. This example clearly shows
531 that molecular-level studies allow systematic understanding of ion retention that occurs in
532 natural systems, and to develop its application such as extraction of useful metals.

533 Retention reversibility and adsorbed cation mobility are two key aspects of resources extraction
534 efficiency in industrial processes and contaminant mobility in pollution control engineering.
535 Both properties are linked with the speciation of metal cations at clay mineral surfaces, with
536 the presence of outer-sphere complexes enhancing reversibility and mobility.

537 **[H1] Summary and future directions**

538 The accurate predictions of metal ion – clay mineral interactions over long time- and large-
539 spatial scales in natural and engineered systems necessitates the development of a continuum
540 of macroscopic models that are able to consider a large range of environmental conditions, as
541 well as temporal and spatial changes. Such predictions are currently hampered by the diversity
542 of interaction processes of metal ions with clay mineral surfaces, and by the difficulty to
543 unravel their respective contributions in the results of macroscopic experiments that are used
544 to calibrate retention models, such as surface complexation models. This limitation is currently
545 being addressed by implementing retention models with molecular level characterization to
546 better understand adsorption and related processes.

547 The highly complex nature of clay mineral-metal ion interactions requires the application of
548 multiple techniques to reach insightful conclusions. Important progress has been made since
549 the ~2000s in this direction, with important breakthroughs in deciphering mechanisms of
550 adsorption and of incorporation of elements, with applications to the formation mechanisms of
551 economically important metal deposits, as well as to the containment of hazardous materials
552 by clay-rich barriers. Since the 2010s, the emerging coupling of quantum mechanics simulation
553 predictions with molecular level synchrotron-based characterization techniques proved to be
554 very powerful to better constrain the nature and location of adsorption sites, binding
555 mechanisms, as well as the energy associated to binding reactions, thus allowing further
556 development of macroscopic models with a reduced number of empirically fitted parameters.
557 It is now also possible to obtain quantified information on surface nucleation and growth
558 mechanisms that are yet not integrated into geochemical modelling approaches.

559 With the application of higher quantum mechanical levels (such as advanced density functional
560 and perturbation theory), more accurate estimates can be made, approaching chemical accuracy
561 (about 1 kJ mol⁻¹). Multiscale modelling will allow the system size and time scale to be
562 expanded substantially towards ~µm and ~s respectively, enabling the direct simulation of slow
563 processes, such as nucleation and dissolution, and promoting the combination with
564 experimental results. Therefore, one can expect that the continuous development of efficient
565 algorithms and increases in computing power will greatly advance the predictive capability of

566 microscopic simulation, which is going to play an ever more important role in guiding
567 industrial and engineering applications.

568 Concerning adsorption processes, the quantification of surface ternary complex formation (in
569 particular, in the presence of carbonated metal ions species) and a better understanding of
570 metal-organic matter-clay mineral surface interactions, are needed to model conditions relevant
571 to natural systems. Surface nucleation and growth clearly deserves more mechanistic research
572 for their fundamental importance in both pollution control engineering and transition metal
573 enriched clay deposits, such as zinc clay ores¹¹⁸ and nickel laterite ores²¹⁴.

574 Surface induced redox reactions have important implications for the containment performance
575 of engineered and natural clay-rich barriers in pollution control applications, but also for
576 bioremediation applications. The detailed understanding of surface induced redox reactions
577 with respect to the retention of redox sensitive metals still requires extensive research before
578 implementation in geochemical models, particularly with respect to the redox properties of
579 iron. In particular, further research is needed for the identification of electron transfer paths
580 and efficiency; for the assessment and thermodynamic description of intrinsic redox potential
581 of structural and adsorbed Fe; for the identification of relationship between changes in Fe
582 oxidation state and surface chemistry; and, for the quantification of Fe redox reactivity as a
583 function of its abundance and location in the crystal structure.

584 The growing scientific interest in the quantification and understanding of clay mineral retention
585 properties must be put in perspective with industrial and environmental applications that rely
586 on the ability of clay minerals to scavenge metal ions. Bulk characterization of retention
587 properties is necessary to study the effectiveness of clay-rich materials for such applications,
588 but still is not sufficient to quantify these processes over long timescales. Process
589 understanding at the molecular level combined with multiscale simulation approaches has
590 proved to be essential to predict parameters such as resource extractability and contaminant
591 mobility.

References:

- 594 1. Bergaya, F. & Lagaly, G. *Handbook of clay science, second edition. 1 and 2*, (Elsevier:
595 2013).
- 596 2. Sposito, G., Skipper, N. T., Sutton, R., Park, S. & Soper, A. K. Surface geochemistry of the
597 clay minerals. *Proceedings of the National Academy of Sciences of the United States of*
598 *America* **96**, 3358–3364 (1999).
- 599 3. Li, M. Y. H. & Zhou, M.-F. The role of clay minerals in formation of the regolith-hosted
600 heavy rare earth element deposits. **105**, 92–108 (2020).
- 601 4. Delay, J., Distinguin, M. & Dewonck, S. Characterization of a clay-rich rock through
602 development and installation of specific hydrogeological and diffusion test equipment
603 in deep boreholes. *Physics and Chemistry of the Earth, Parts A/B/C* **32**, 393–407 (2007).
- 604 5. Mishra, H., Karmakar, S., Kumar, R. & Kadambala, P. A long-term comparative
605 assessment of human health risk to leachate-contaminated groundwater from heavy
606 metal with different liner systems. **25**, 2911–2923 (2018).
- 607 6. Yi, X. *et al.* Remediation of heavy metal-polluted agricultural soils using clay minerals: a
608 review. **27**, 193–204 (2017).
- 609 7. Brigatti, M. F., Galán, E. & Theng, B. K. G. Chapter 2 - Structure and Mineralogy of Clay
610 Minerals. *Handbook of Clay Science* **5**, 21–81 (2013).
- 611 8. Yuan, G. D., Theng, B. K. G., Churchman, G. J. & Gates, W. P. Chapter 5.1 - Clays and Clay
612 Minerals for Pollution Control. *Handbook of Clay Science* **5**, 587–644 (2013).
- 613 9. Altmann, S. Geochemical research: A key building block for nuclear waste disposal
614 safety cases. *Journal of Contaminant Hydrology* **102**, 174–179 (2008).
- 615 10. Skipper, N., Soper, A. & McConnell, J. The structure of interlayer water in vermiculite.
616 **94**, 5751–5760 (1991).
- 617 11. Schlegel, M. L. *et al.* Cation sorption on the muscovite (0 0 1) surface in chloride
618 solutions using high-resolution X-ray reflectivity. *Geochimica et Cosmochimica Acta* **70**,
619 3549–3565 (2006).
- 620 12. Dähn, R. *et al.* Neof ormation of Ni phyllosilicate upon Ni uptake on montmorillonite: a
621 kinetics study by powder and polarized extended X-ray absorption fine structure
622 spectroscopy. *Geochimica et Cosmochimica Acta* **66**, 2335–2347 (2002).
- 623 13. Manceau, A. & Calas, G. Nickel-bearing clay minerals: II. Intracrystalline distribution of
624 nickel: an X-ray absorption study. **21**, 341–360 (1986).
- 625 14. Churakov, S. V. & Prasianakis, N. I. Review of the current status and challenges for a
626 holistic process-based description of mass transport and mineral reactivity in porous
627 media. *American Journal of Science* **318**, 921–948 (2018).
- 628 15. Churakov, S. V. & Gimmi, T. Up-scaling of molecular diffusion coefficients in clays: A two-
629 step approach. *The Journal of Physical Chemistry C* **115**, 6703–6714 (2011).
- 630 16. Brouwer, E., Baeyens, B., Maes, A. & Cremers, A. Cesium and Rubidium ion equilibria in
631 illite clay. *Journal of Physical Chemistry* **87**, 1213–1219 (1983).
- 632 17. De Koning, A. & Comans, R. N. J. Reversibility of radiocaesium sorption on illite.
633 *Geochimica et Cosmochimica Acta* **68**, 2815–2823 (2004).

- 634 18. Poinssot, C., Baeyens, B. & Bradbury, M. H. *Experimental studies of Cs, Sr, Ni, and Eu*
635 *sorption on Na-illite and the modelling of Cs sorption*. (Paul Scherrer Institut: 1999).
- 636 19. Verburg, K. & Baveye, P. Hysteresis in the binary exchange of cations on 2/1 clay-
637 minerals - a critical-review. *Clays and Clay Minerals* **42**, 207–220 (1994).
- 638 20. Comans, R. N. J., Haller, M. & De Preter, P. Sorption of cesium on illite: Non-equilibrium
639 behaviour and reversibility. *Geochimica et Cosmochimica Acta* **55**, 433–440 (1991).
- 640 21. Oscarson, D. W., Hume, H. B. & King, F. Sorption of cesium on compacted bentonite.
641 *Clays and Clay Minerals* **42**, 731–736 (1994).
- 642 22. Bellenger, J. P. & Staunton, S. Adsorption and desorption of Sr-85 and Cs-137 on
643 reference minerals, with and without inorganic and organic surface coatings. *Journal of*
644 *Environmental Radioactivity* **99**, 831–840 (2008).
- 645 23. Dyer, A., Chow, J. K. & Umar, I. M. The uptake of caesium and strontium radioisotopes
646 onto clays. *Journal of Materials Chemistry* **10**, 2734–2740 (2000).
- 647 24. Baeyens, B. & Bradbury, M. H. A mechanistic description of Ni and Zn sorption on Na-
648 montmorillonite. Part I: Titration and sorption measurements. *Journal of Contaminant*
649 *Hydrology* **27**, 199–222 (1997).
- 650 25. Gu, X. & Evans, L. J. Modelling the adsorption of Cd(II), Cu(II), Ni(II), Pb(II), and Zn(II)
651 onto Fithian illite. *Journal of Colloid and Interface Science* **307**, 317–325 (2007).
- 652 26. Bradbury, M. H. & Baeyens, B. Sorption modelling on illite Part I: Titration
653 measurements and the sorption of Ni, Co, Eu and Sn. *Geochimica et Cosmochimica Acta*
654 **73**, 990–1003 (2009).
- 655 27. Bradbury, M. H. & Baeyens, B. Modelling the sorption of Mn(II), Co(II), Ni(II), Zn(II),
656 Cd(II), Eu(III), Am(III), Sn(IV), Th(IV), Np(V) and U(VI) on montmorillonite: Linear free
657 energy relationships and estimates of surface binding constants for some selected
658 heavy metals and actinides. *Geochimica et Cosmochimica Acta* **69**, 875–892 (2005).
- 659 28. Akafia, M. M., Reich, T. J. & Koretsky, C. M. Assessing Cd, Co, Cu, Ni, and Pb Sorption on
660 montmorillonite using surface complexation models. *Applied geochemistry* **26**, S154–
661 S157 (2011).
- 662 29. Marques Fernandes, M., Scheinost, A. & Baeyens, B. Sorption of trivalent lanthanides
663 and actinides onto montmorillonite: Macroscopic, thermodynamic and structural
664 evidence for ternary hydroxo and carbonato surface complexes on multiple sorption
665 sites. *Water Research* **99**, 74–82 (2016).
- 666 30. Bradbury, M. H. & Baeyens, B. Sorption modelling on illite. Part II: Actinide sorption and
667 linear free energy relationships. *Geochimica et Cosmochimica Acta* **73**, 1004–1013
668 (2009).
- 669 31. Bradbury, M. H. & Baeyens, B. Experimental measurements and modeling of sorption
670 competition on montmorillonite. *Geochimica et Cosmochimica Acta* **69**, 4187–4197
671 (2005).
- 672 32. Grangeon, S. *et al.* The influence of natural trace element distribution on the mobility
673 of radionuclides. The exemple of nickel in a clay-rock. *Applied Geochemistry* **52**, 155–
674 173 (2015).
- 675 33. Marques Fernandes, M. & Baeyens, B. Cation exchange and surface complexation of
676 lead on montmorillonite and illite including competitive adsorption effects. *Applied*
677 *Geochemistry* **100**, 190–202 (2019).
- 678 34. Gao, Y., Shao, Z. & Xiao, Z. U (VI) sorption on illite: effect of pH, ionic strength, humic
679 acid and temperature. *Journal of Radioanalytical and Nuclear Chemistry* **303**, 867–876
680 (2015).

- 681 35. Uddin, M. K. A review on the adsorption of heavy metals by clay minerals, with special
682 focus on the past decade. *Chemical Engineering Journal* **308**, 438–462 (2017).
- 683 36. Goldberg, S. & Glaubig, R. A. Anion sorption on a calcareous, montmorillonitic soil-
684 selenium. *Soil Science Society of America Journal* **52**, 954–958 (1988).
- 685 37. Palmer, D. A. & Meyer, R. E. Adsorption of technetium on selected inorganic ion-
686 exchange materials and on a range of naturally occurring minerals under oxic
687 conditions. *Journal of Inorganic and Nuclear Chemistry* **43**, 2979–2984 (1981).
- 688 38. Missana, T., Alonso, U. & Garcia-Gutiérrez, M. Experimental study and modelling of
689 selenite sorption onto illite and smectite clays. *Journal of Colloid and Interface Science*
690 **334**, 132–138 (2009).
- 691 39. Peak, D., Saha, U. & Huang, P. Selenite adsorption mechanisms on pure and coated
692 montmorillonite: an EXAFS and XANES spectroscopic study. **70**, 192–203 (2006).
- 693 40. Ervanne, H., Hakanen, M. & Lehto, J. Selenium sorption on clays in synthetic
694 groundwaters representing crystalline bedrock conditions. **307**, 1365–1373 (2016).
- 695 41. Goldberg, S. Modeling selenite adsorption envelopes on oxides, clay minerals, and soils
696 using the triple layer model. **77**, 64–71 (2013).
- 697 42. Manning, B. A. & Goldberg, S. Adsorption and stability of arsenic(III) at the clay mineral-
698 water interface. *Environmental Science & Technology* **31**, 2005–2011 (1997).
- 699 43. Garcia-Sanchez, A., Alvarez-Ayuso, E. & Rodriguez-Martin, F. Sorption of As (V) by some
700 oxyhydroxides and clay minerals. Application to its immobilization in two polluted
701 mining soils. **37**, 187–194 (2002).
- 702 44. Mohapatra, D., Mishra, D., Chaudhury, G. R. & Das, R. Arsenic (V) adsorption mechanism
703 using kaolinite, montmorillonite and illite from aqueous medium. **42**, 463–469 (2007).
- 704 45. Goldberg, S. Competitive adsorption of arsenate and arsenite on oxides and clay
705 minerals. **66**, 413–421 (2002).
- 706 46. Xi, J., He, M. & Lin, C. Adsorption of antimony (III) and antimony (V) on bentonite:
707 kinetics, thermodynamics and anion competition. **97**, 85–91 (2011).
- 708 47. Goldberg, S., Forster, H. & Godfrey, C. Molybdenum adsorption on oxides, clay minerals,
709 and soils. *Soil Science Society of America Journal* **60**, 425–432 (1996).
- 710 48. Lee, S. M. & Tiwari, D. Organo and inorgano-organo-modified clays in the remediation
711 of aqueous solutions: An overview. *Applied Clay Science* **59**, 84–102 (2012).
- 712 49. Fletcher, P. & Sposito, G. The chemical modeling of clay/electrolyte interactions for
713 montmorillonite. *Clay Minerals* **24**, 375–391 (1989).
- 714 50. Bradbury, M. H. & Baeyens, B. A mechanistic description of Ni and Zn sorption on Na-
715 montmorillonite. Part II: modeling. *Journal of Contaminant Hydrology* **27**, 223–248
716 (1997).
- 717 51. Loganathan, N. & Kalinichev, A. G. Quantifying the mechanisms of site-specific ion
718 exchange at an inhomogeneously charged surface: Case of Cs⁺/K⁺ on hydrated
719 muscovite mica. *The Journal of Physical Chemistry C* **121**, 7829–7836 (2017).
- 720 52. Loganathan, N., Yazaydin, A. O., Bowers, G. M., Kalinichev, A. G. & Kirkpatrick, R. J.
721 Structure, energetics, and dynamics of Cs⁺ and H₂O in hectorite: Molecular dynamics
722 simulations with an unconstrained substrate surface. *The Journal of Physical Chemistry*
723 *C* **120**, 10298–10310 (2016).
- 724 53. Liu, X., Lu, X., Wang, R. & Zhou, H. Effects of layer-charge distribution on the
725 thermodynamic and microscopic properties of Cs-smectite. *Geochimica et*
726 *Cosmochimica Acta* **72**, 1837–1847 (2008).

- 727 54. Tournassat, C., Grangeon, S., Leroy, P. & Giffaut, E. Modeling specific pH dependent
728 sorption of divalent metals on montmorillonite surfaces. A review of pitfalls, recent
729 achievements and current challenges. *American Journal of Science* **313**, 395–451 (2013).
- 730 55. Thomas, H. C. & Gaines, G. L. J. The thermodynamics of ion exchange on clay minerals.
731 A preliminary report on the system montmorillonite-Cs-Sr. *Clays and Clay Minerals* **2**,
732 398–403 (1953).
- 733 56. Vanselow, A. P. The utilization of the base-exchange reaction for the determination of
734 activity coefficients in mixed electrolytes. *Journal of American Chemical Society* **54**,
735 1307–1311 (1932).
- 736 57. Bourg, I. C. & Sposito, G. Ion exchange phenomena. *Handbook of Soil Science, second*
737 *edition* (2011).
- 738 58. Tournassat, C. *et al.* Cation exchange selectivity coefficient values on smectite and
739 mixed-layer illite/smectite minerals. *Soil Science Society of America Journal* **73**, 928–942
740 (2009).
- 741 59. Lammers, L. N. *et al.* Molecular dynamics simulations of cesium adsorption on illite
742 nanoparticles. *Journal of Colloid and Interface Science* **submitted**, (2016).
- 743 60. Poinssot, C., Baeyens, B. & Bradbury, M. H. Experimental and modelling studies of
744 caesium sorption on illite. *Geochimica et Cosmochimica Acta* **63**, 3217–3227 (1999).
- 745 61. Bergaoui, L., Lambert, J. F. & Prost, R. Cesium adsorption on soil clay: macroscopic and
746 spectroscopic measurements. *Applied Clay Science* **29**, 23–29 (2005).
- 747 62. Meleshyn, A. Adsorption of Sr²⁺ and Ba²⁺ at the cleaved mica–water interface: Free
748 energy profiles and interfacial structure. *Geochimica et Cosmochimica Acta* **74**, 1485–
749 1497 (2010).
- 750 63. Bourg, I. C., Lee, S. S., Fenter, P. & Tournassat, C. Stern Layer Structure and Energetics
751 at Mica–Water Interfaces. *The Journal of Physical Chemistry C* **121**, 9402–9412 (2017).
- 752 64. Zaunbrecher, L. K., Cygan, R. T. & Elliott, W. C. Molecular models of cesium and rubidium
753 adsorption on weathered micaceous minerals. *The Journal of Physical Chemistry A* **119**,
754 5691–5700 (2015).
- 755 65. Rotenberg, B., Marry, V., Malikova, N. & Turq, P. Molecular simulation of aqueous
756 solutions at clay surfaces. *Journal of Physics: Condensed Matter* **22**, 284114 (2010).
- 757 66. Tournassat, C., Chapron, Y., Leroy, P. & Boulahya, F. Comparison of molecular dynamics
758 simulations with Triple Layer and modified Gouy-Chapman models in a 0.1 M NaCl -
759 montmorillonite system. *Journal of Colloid and Interface Science* **339**, 533–541 (2009).
- 760 67. Li, X., Liu, N. & Zhang, J. Adsorption of cesium at the external surface of TOT type clay
761 mineral: effect of the interlayer cation and the hydrated state. **123**, 19540–19548
762 (2019).
- 763 68. Tournassat, C., Bourg, I. C., Steefel, C. I. & Bergaya, F. Chapter 1 - Surface Properties of
764 Clay Minerals. *Natural and Engineered Clay Barriers* **6**, 5–31 (2015).
- 765 69. Liu, L. Prediction of swelling pressures of different types of bentonite in dilute solutions.
766 *Colloids and Surfaces A: Physicochemical and Engineering Aspects* **434**, 303–318 (2013).
- 767 70. Van Loon, L. R. & Glaus, M. A. Mechanical compaction of smectite clays increases ion
768 exchange selectivity for cesium. *Environmental Science & Technology* **42**, 1600–1604
769 (2008).
- 770 71. Rotenberg, B., Morel, J.-P., Marry, V., Turq, P. & Morel-Desrosiers, N. On the driving
771 force of cation exchange in clays: Insights from combined microcalorimetry experiments
772 and molecular simulation. *Geochimica et Cosmochimica Acta* **73**, 4034–4044 (2009).

- 773 72. Teppen, B. J. & Miller, D. M. Hydration energy determines isovalent cation exchange
774 selectivity by clay minerals. *Soil Science Society of America Journal* **70**, 31–40 (2006).
- 775 73. Cygan, R. T., Greathouse, J. A. & Kalinichev, A. G. Advances in Clayff molecular
776 simulation of layered and nanoporous materials and their aqueous interfaces. **125**,
777 17573–17589 (2021).
- 778 74. Le Crom, S., Tournassat, C., Robinet, J.-C. & Marry, V. Influence of polarisability on the
779 prediction of the electrical double layer structure in a clay mesopore: A molecular
780 dynamics study. *The Journal of Physical Chemistry C* **124**, 6221–6232 (2020).
- 781 75. Tesson, S. *et al.* Classical polarizable force field to study hydrated charged clays and
782 zeolites. **122**, 24690–24704 (2018).
- 783 76. Churakov, S. V. Mobility of Na and Cs on montmorillonite surface under partially
784 saturated conditions. *Environmental Science & Technology* **47**, 9816–9823 (2013).
- 785 77. Simonnin, P., Marry, V., Noetinger, B., Nieto-Draghi, C. & Rotenberg, B. Mineral-and ion-
786 specific effects at clay–water interfaces: structure, diffusion, and hydrodynamics. *The*
787 *Journal of Physical Chemistry C* **122**, 18484–18492 (2018).
- 788 78. Malikova, N., Dubois, E., Marry, V., Rotenberg, B. & Turq, P. Dynamics in clays-combining
789 neutron scattering and microscopic simulation. **224**, 153–181 (2010).
- 790 79. Porion, P. *et al.* 133Cs Nuclear Magnetic Resonance relaxometry as a probe of the
791 mobility of cesium cations confined within dense clay sediments. **119**, 15360–15372
792 (2015).
- 793 80. Appelo, C. A. J., Van Loon, L. R. & Wersin, P. Multicomponent diffusion of a suite of
794 tracers (HTO, Cl, Br, I, Na, Sr, Cs) in a single sample of Opalinus clay. *Geochimica et*
795 *Cosmochimica Acta* **74**, 1201–1219 (2010).
- 796 81. Churakov, S. V., Gimmi, T., Unruh, T., Van Loon, L. R. & Juranyi, F. Resolving diffusion in
797 clay minerals at different time scales: Combination of experimental and modeling
798 approaches. *Applied Clay Science* (2014).
- 799 82. Tournassat, C. & Steefel, C. I. Reactive transport modeling of coupled processes in
800 nanoporous media. *Reviews in Mineralogy and Geochemistry* **85**, 75–110 (2019).
- 801 83. Altmann, S. *et al.* Diffusion-driven transport in clayrock formations. *Applied*
802 *Geochemistry* **27**, 463–478 (2012).
- 803 84. Charlet, L., Alt-Epping, P., Wersin, P. & Gilbert, B. Diffusive transport and reaction in clay
804 rocks: A storage (nuclear waste, CO₂, H₂), energy (shale gas) and water quality issue.
805 *Advances in Water Resources* **106**, 39–59 (2017).
- 806 85. Grambow, B. Geological disposal of radioactive waste in clay. *Elements* **12**, 239–245
807 (2016).
- 808 86. Whittaker, M. L., Lammers, L. N., Carrero, S., Gilbert, B. & Banfield, J. F. Ion exchange
809 selectivity in clay is controlled by nanoscale chemical–mechanical coupling. *Proceedings*
810 *of the National Academy of Sciences* **116**, 22052–22057 (2019).
- 811 87. Liu, X., Cheng, J., Sprik, M., Lu, X. & Wang, R. Interfacial structures and acidity of edge
812 surfaces of ferruginous smectites. *Geochimica et Cosmochimica Acta* **168**, 293–301
813 (2015).
- 814 88. Liu, X., Cheng, J., Sprik, M., Lu, X. & Wang, R. Surface acidity of 2:1-type dioctahedral
815 clay minerals from first principles molecular dynamics simulations. *Geochimica et*
816 *Cosmochimica Acta* **140**, 410–417 (2014).
- 817 89. Liu, X. *et al.* Acidity of edge surface sites of montmorillonite and kaolinite. *Geochimica*
818 *et Cosmochimica Acta* **117**, 180–190 (2013).

- 819 90. Genuchten, C. M. van & Peña, J. Antimonate and arsenate speciation on reactive soil
820 minerals studied by differential pair distribution function analysis. *Chemical Geology*
821 **429**, 1–9 (2016).
- 822 91. Dähn, R. *et al.* Structural evidence for the sorption of Ni(II) atoms on the edges of
823 montmorillonite clay minerals: A polarized X-ray absorption fine structure study.
824 *Geochimica et Cosmochimica Acta* **37**, 1–15 (2003).
- 825 92. Dähn, R., Baeyens, B. & Bradbury, M. H. Investigation of the different binding edge sites
826 for Zn on montmorillonite using P-EXAFS - The strong/weak site concept in the 2SPNE
827 SC/CE sorption model. *Geochimica et Cosmochimica Acta* **75**, 5154–5168 (2011).
- 828 93. Churakov, S. V. & Dähn, R. Zinc Adsorption on Clays Inferred from Atomistic Simulations
829 and EXAFS Spectroscopy. *Environmental Science & Technology* **46**, 5713–5719 (2012).
- 830 94. Rabung, T. *et al.* Sorption of Eu(III)/Cm(III) on Ca-montmorillonite and Na-illite. Part 1:
831 Batch sorption and time-resolved laser fluorescence spectroscopy experiments.
832 *Geochimica et Cosmochimica Acta* **69**, 5393–5402 (2005).
- 833 95. Sasaki, T. *et al.* Sorption of Eu³⁺ on Na-montmorillonite studied by time-resolved laser
834 fluorescence spectroscopy and surface complexation modeling. *Journal of Nuclear*
835 *Science and Technology* **53**, 592–601 (2016).
- 836 96. Verma, P. K. *et al.* Eu (III) sorption onto various montmorillonites: Experiments and
837 modeling. *Applied Clay Science* **175**, 22–29 (2019).
- 838 97. Zhang, C. *et al.* Cadmium (II) complexes adsorbed on clay edge surfaces: Insight from
839 first principles molecular dynamics simulation. *Clays and Clay Minerals* **64**, 337–347
840 (2016).
- 841 98. Zhang, C. *et al.* Surface complexation of heavy metal cations on clay edges: insights from
842 first principles molecular dynamics simulation of Ni (II). *Geochimica et Cosmochimica*
843 *Acta* **203**, 54–68 (2017).
- 844 99. Tournassat, C., Tinnacher, R. M., Grangeon, S. & Davis, J. A. Modeling uranium (VI)
845 adsorption onto montmorillonite under varying carbonate concentrations: A surface
846 complexation model accounting for the spillover effect on surface potential.
847 *Geochimica et Cosmochimica Acta* **220**, 291–308 (2018).
- 848 100. Marques Fernandes, M., Baeyens, B., Dähn, R., Scheinost, A. & Bradbury, M. U(VI)
849 sorption on montmorillonite in the absence and presence of carbonate: A macroscopic
850 and microscopic study. **93**, 262–277 (2012).
- 851 101. Kremleva, A., Martorell, B., Krüger, S. & Rösch, N. Uranyl adsorption on solvated edge
852 surfaces of pyrophyllite: a DFT model study. *Physical Chemistry Chemical Physics* **14**,
853 5815–5823 (2012).
- 854 102. Kremleva, A., Krüger, S. & Rösch, N. Uranyl adsorption at solvated edge surfaces of 2: 1
855 smectites. A density functional study. *Physical Chemistry Chemical Physics* **17**, 13757–
856 13768 (2015).
- 857 103. Kremleva, A., Krüger, S. & Rösch, N. Toward a reliable energetics of adsorption at
858 solvated mineral surfaces: A computational study of uranyl (VI) on 2: 1 clay minerals.
859 *The Journal of Physical Chemistry C* **120**, 324–335 (2016).
- 860 104. Zhang, C., Liu, X., Tinnacher, R. M. & Tournassat, C. Mechanistic understanding of uranyl
861 ion complexation on montmorillonite edges: A combined first-principles molecular
862 dynamics - surface complexation modeling approach. *Environmental Science &*
863 *Technology* **52**, 8501–8509 (2018).

- 864 105. Catalano, J. G. & Brown, G. E. Jr. Uranyl adsorption onto montmorillonite: Evaluation of
865 binding sites and carbonate complexation. *Geochimica et Cosmochimica Acta* **69**, 2995–
866 3005 (2005).
- 867 106. Schlegel, M. L. & Descostes, M. Uranium uptake by hectorite and montmorillonite: a
868 solution chemistry and polarized EXAFS study. *Environmental Science & Technology* **43**,
869 8593–8598 (2009).
- 870 107. Ford, R. G. & Sparks, D. L. The nature of Zn precipitates formed in the presence of
871 pyrophyllite. *Environmental Science and Technology* **34**, 2479–2483 (2000).
- 872 108. Schlegel, M. L. & Manceau, A. Evidence for the nucleation and epitaxial growth of Zn
873 phyllosilicate on montmorillonite. *Geochimica et Cosmochimica Acta* **70**, 901–917
874 (2006).
- 875 109. Scheidegger, A. M., Lamble, G. M. & Sparks, D. L. Spectroscopic evidence for the
876 formation of mixed-cation hydroxide phases upon metal sorption on clays and
877 aluminum oxides. *Journal of Colloid and Interface Science* **186**, 118–128 (1997).
- 878 110. Siebecker, M., Li, W., Khalid, S. & Sparks, D. Real-time QEXAFS spectroscopy measures
879 rapid precipitate formation at the mineral–water interface. *Nature communications* **5**,
880 1–7 (2014).
- 881 111. Thompson, H. A., Parks, G. A. & Brown Jr., G. E. Dynamic interactions of dissolution,
882 surface adsorption, and precipitation in an aging cobalt(II)-clay-water system.
883 *Geochimica et Cosmochimica Acta* **63**, 1767–1779 (1999).
- 884 112. Starcher, A. N., Li, W., Kukkadapu, R. K., Elzinga, E. J. & Sparks, D. L. Fe (II) sorption on
885 pyrophyllite: Effect of structural Fe (III)(impurity) in pyrophyllite on nature of layered
886 double hydroxide (LDH) secondary mineral formation. *Chemical Geology* **439**, 152–160
887 (2016).
- 888 113. Zhu, Y. & Elzinga, E. J. Formation of layered Fe(II)-hydroxides during Fe(II) sorption onto
889 clay and metal-oxide substrates. *Environmental science & technology* **48**, 4937–4945
890 (2014).
- 891 114. Zhang, C., Liu, X., Lu, X., Meijer, E. J. & Wang, R. Understanding the Heterogeneous
892 Nucleation of Heavy Metal Phyllosilicates on Clay Edges with First-Principles Molecular
893 Dynamics. *Environmental science & technology* **53**, 13704–13712 (2019).
- 894 115. Jacquat, O., Voegelin, A., Villard, A., Marcus, M. A. & Kretzschmar, R. Formation of Zn-
895 rich phyllosilicate, Zn-layered double hydroxide and hydrozincite in contaminated
896 calcareous soils. *Geochimica et Cosmochimica Acta* **72**, 5037–5054 (2008).
- 897 116. Choulet, F., Buatier, M., Barbanson, L., Guégan, R. & Ennaciri, A. Zinc-rich clays in
898 supergene non-sulfide zinc deposits. *Mineralium Deposita* **51**, 467–490 (2016).
- 899 117. Roqué-Rosell, J., Villanova-de-Benavent, C. & Proenza, J. A. The accumulation of Ni in
900 serpentines and garnierites from the Falcondo Ni-laterite deposit (Dominican Republic)
901 elucidated by means of μ XAS. *Geochimica et Cosmochimica Acta* **198**, 48–69 (2017).
- 902 118. Balassone, G., Nieto, F., Arfè, G., Boni, M. & Mondillo, N. Zn-clay minerals in the
903 Skorpion Zn nonsulfide deposit (Namibia): Identification and genetic clues revealed by
904 HRTEM and AEM study. *Applied Clay Science* **150**, 309–322 (2017).
- 905 119. Chassé, M., Griffin, W. L., O'Reilly, S. Y. & Calas, G. Australian laterites reveal
906 mechanisms governing scandium dynamics in the critical zone. *Geochimica et*
907 *Cosmochimica Acta* **260**, 292–310 (2019).
- 908 120. Stucki, J. W. Chapter 11 - Properties and Behaviour of Iron in Clay Minerals. *Handbook*
909 *of Clay Science* **5**, 559–611 (2013).
- 910 121. Huang, J. *et al.* Fe (II) Redox Chemistry in the Environment. (2021).

- 911 122. Chakraborty, S. *et al.* U(VI) Sorption and Reduction by Fe(II) Sorbed on Montmorillonite.
912 *Environmental Science & Technology* **44**, 3779–3785 (2010).
- 913 123. Liger, E., Charlet, L. & Van Cappellen, P. Surface catalysis of uranium (VI) reduction by
914 iron(II). *Geochimica Cosmochimica Acta* **63**, 2939–2955 (1999).
- 915 124. Brookshaw, D. R. *et al.* Redox interactions of Tc (VII), U (VI), and Np (V) with microbially
916 reduced biotite and chlorite. *Environmental science & technology* **49**, 13139–13148
917 (2015).
- 918 125. Begg, J. D., Edelman, C., Zavarin, M. & Kersting, A. B. Sorption kinetics of plutonium
919 (V)/(VI) to three montmorillonite clays. **96**, 131–137 (2018).
- 920 126. Hixon, A. E. & Powell, B. A. Plutonium environmental chemistry: mechanisms for the
921 surface-mediated reduction of Pu (v/vi). **20**, 1306–1322 (2018).
- 922 127. Charlet, L. *et al.* Electron transfer at the mineral/water interface: Selenium reduction by
923 ferrous iron sorbed on clay. *Geochimica et Cosmochimica Acta* **71**, 5731–5749 (2007).
- 924 128. Ilgen, A. G., Krulichak, J. N., Artyushkova, K., Newville, M. G. & Sun, C. Redox
925 transformations of As and Se at the surfaces of natural and synthetic ferric nontronites:
926 role of structural and adsorbed Fe (II). *Environmental science & technology* **51**, 11105–
927 11114 (2017).
- 928 129. Bishop, M. E., Dong, H., Kukkadapu, R. K., Liu, C. & Edlmann, R. E. Bioreduction of Fe-
929 bearing clay minerals and their reactivity toward pertechnetate (Tc-99). *Geochimica et*
930 *Cosmochimica Acta* **75**, 5229–5246 (2011).
- 931 130. Jaisi, D. P. *et al.* Reduction and long-term immobilization of technetium by Fe (II)
932 associated with clay mineral nontronite. *Chemical Geology* **264**, 127–138 (2009).
- 933 131. Qafoku, O. *et al.* Tc (VII) and Cr (VI) interaction with naturally reduced ferruginous
934 smectite from a redox transition zone. *Environmental science & technology* **51**, 9042–
935 9052 (2017).
- 936 132. Brigatti, M. F. *et al.* Reduction and sorption of chromium by Fe(II)-bearing
937 phyllosilicates: chemical treatments and X-ray absorption spectroscopy (XAS) studies.
938 *Clays and Clay Minerals* **48**, 272–281 (2000).
- 939 133. Joe-Wong, C., Brown Jr, G. E. & Maher, K. Kinetics and products of chromium (VI)
940 reduction by iron (II/III)-bearing clay minerals. *Environmental science & technology* **51**,
941 9817–9825 (2017).
- 942 134. Liao, W. *et al.* Effect of coexisting Fe (III)(oxyhydr) oxides on Cr (VI) reduction by Fe (II)-
943 bearing clay minerals. *Environmental science & technology* **53**, 13767–13775 (2019).
- 944 135. Bishop, M. E., Glasser, P., Dong, H., Arey, B. & Kovarik, L. Reduction and immobilization
945 of hexavalent chromium by microbially reduced Fe-bearing clay minerals. *Geochimica*
946 *et Cosmochimica Acta* **133**, 186–203 (2014).
- 947 136. Scheinost, A. C. *et al.* X-ray absorption and photoelectron spectroscopy investigation of
948 selenite reduction by Fe-II-bearing minerals. *Journal of Contaminant Hydrology* **102**,
949 228–245 (2008).
- 950 137. Ilgen, A. G., Foster, A. L. & Trainor, T. P. Role of structural Fe in nontronite NAu-1 and
951 dissolved Fe (II) in redox transformations of arsenic and antimony. *Geochimica et*
952 *Cosmochimica Acta* **94**, 128–145 (2012).
- 953 138. Cheng, J. & Sprik, M. Alignment of electronic energy levels at electrochemical interfaces.
954 *Physical Chemistry Chemical Physics* **14**, 11245–11267 (2012).
- 955 139. Blumberger, J. Recent advances in the theory and molecular simulation of biological
956 electron transfer reactions. *Chemical reviews* **115**, 11191–11238 (2015).

- 957 140. Cheng, J., Liu, X., Kattirtzi, J. A., VandeVondele, J. & Sprik, M. Aligning Electronic and
958 Protonic Energy Levels of Proton-Coupled Electron Transfer in Water Oxidation on
959 Aqueous TiO₂. *Angewandte Chemie* **126**, 12242–12246 (2014).
- 960 141. Anisimov, V. I., Zaanen, J. & Andersen, O. K. Band theory and Mott insulators: Hubbard
961 U instead of Stoner I. *Physical Review B* **44**, 943 (1991).
- 962 142. Behler, J., Delley, B., Reuter, K. & Scheffler, M. Nonadiabatic potential-energy surfaces
963 by constrained density-functional theory. *Physical Review B* **75**, 115409 (2007).
- 964 143. Alexandrov, V. & Rosso, K. M. Insights into the mechanism of Fe (II) adsorption and
965 oxidation at Fe–Clay mineral surfaces from first-principles calculations. *The Journal of*
966 *Physical Chemistry C* **117**, 22880–22886 (2013).
- 967 144. Liu, X., Cheng, J. & Sprik, M. Aqueous transition-metal cations as impurities in a wide
968 gap oxide: The Cu²⁺/Cu⁺ and Ag²⁺/Ag⁺ redox couples revisited. *The Journal of Physical*
969 *Chemistry B* **119**, 1152–1163 (2015).
- 970 145. Cheng, J. & VandeVondele, J. Calculation of electrochemical energy levels in water using
971 the random phase approximation and a double hybrid functional. *Physical review letters*
972 **116**, 086402 (2016).
- 973 146. Cheng, J., Liu, X., VandeVondele, J., Sulpizi, M. & Sprik, M. Redox potentials and acidity
974 constants from density functional theory based molecular dynamics. *Accounts of*
975 *chemical research* **47**, 3522–3529 (2014).
- 976 147. Ferrage, E. *et al.* Hydration properties and interlayer organization of water and ions in
977 synthetic Na-smectite with tetrahedral layer charge. Part 2. Toward a precise coupling
978 between molecular simulations and diffraction data. *The Journal of Physical Chemistry*
979 *C* **115**, 1867–1881 (2011).
- 980 148. Tambach, T. J., Hensen, E. J. M. & Smit, B. Molecular simulations of swelling clay
981 minerals. *The Journal of Physical Chemistry B* **108**, 7586–7596 (2004).
- 982 149. Le Crom, S., Tournassat, C., Robinet, J.-C. & Marry, V. Influence of Water Saturation
983 Level on Electrical Double Layer Properties in a Clay Mineral Mesopore: A Molecular
984 Dynamics Study. *The Journal of Physical Chemistry C* (2022).
- 985 150. Savoye, S., Beaucaire, C., Fayette, A., Herbette, M. & Coelho, D. Mobility of cesium
986 through the callovo-oxfordian claystones under partially saturated conditions.
987 *Environmental Science & Technology* **46**, 2633–2641 (2012).
- 988 151. Huang, B. *et al.* Effects of soil particle size on the adsorption, distribution, and migration
989 behaviors of heavy metal (loid) s in soil: a review. *Environmental Science: Processes &*
990 *Impacts* **22**, 1596–1615 (2020).
- 991 152. Kleber, M. *et al.* Mineral–organic associations: formation, properties, and relevance in
992 soil environments. *Advances in agronomy* **130**, 1–140 (2015).
- 993 153. Lagaly, G., Ogawa, M. & Dékény, I. Chapter 10.3 - Clay Mineral - Organic Interactions.
994 *Handbook of Clay Science* **5**, 435–505 (2013).
- 995 154. Kleber, M. *et al.* Dynamic interactions at the mineral–organic matter interface. *Nature*
996 *Reviews Earth & Environment* **2**, 402–421 (2021).
- 997 155. Sutton, R. & Sposito, G. Molecular structure in soil humic substances: the new view.
998 *Environmental science & technology* **39**, 9009–9015 (2005).
- 999 156. Piccolo, A. The supramolecular structure of humic substances. *Soil science* **166**, 810–832
1000 (2001).
- 1001 157. Schnitzer, M. A lifetime perspective on the chemistry of soil organic matter. *Advances*
1002 *in agronomy* **68**, 1–58 (1999).

- 1003 158. Stevenson, F. J. *Humus chemistry: genesis, composition, reactions*. (John Wiley & Sons:
1004 1994).
- 1005 159. Colombo, C. *et al.* Spontaneous aggregation of humic acid observed with AFM at
1006 different pH. *Chemosphere* **138**, 821–828 (2015).
- 1007 160. Kelleher, B. P. & Simpson, A. J. Humic substances in soils: are they really chemically
1008 distinct? *Environmental science & technology* **40**, 4605–4611 (2006).
- 1009 161. Petrov, D., Tunega, D., Gerzabek, M. H. & Oostenbrink, C. Molecular dynamics
1010 simulations of the standard leonardite humic acid: Microscopic analysis of the structure
1011 and dynamics. *Environmental Science & Technology* **51**, 5414–5424 (2017).
- 1012 162. Zhang, Y., Liu, X., Zhang, C. & Lu, X. A combined first principles and classical molecular
1013 dynamics study of clay-soil organic matters (SOMs) interactions. *Geochimica et*
1014 *Cosmochimica Acta* **291**, 110–125 (2020).
- 1015 163. Willemsen, J. A., Myneni, S. C. & Bourg, I. C. Molecular dynamics simulations of the
1016 adsorption of phthalate esters on smectite clay surfaces. *The Journal of Physical*
1017 *Chemistry C* **123**, 13624–13636 (2019).
- 1018 164. Tournassat, C., Steefel, C., Bourg, I. & Bergaya, F. *Natural and engineered clay barriers*.
1019 **6**, (Elsevier: 2015).
- 1020 165. Gates, W. P., Bouazza, A. & Churchman, G. J. Bentonite clay keeps pollutants at bay.
1021 *Elements* **5**, 105–110 (2009).
- 1022 166. Otunola, B. O. & Ololade, O. O. A review on the application of clay minerals as heavy
1023 metal adsorbents for remediation purposes. *Environmental Technology & Innovation*
1024 **18**, 100692 (2020).
- 1025 167. Delage, P., Cui, Y.-J. & Tang, A. M. Clays in radioactive waste disposal. *Journal of Rock*
1026 *Mechanics and Geotechnical Engineering* **2**, 111–123 (2010).
- 1027 168. Mukherjee, S. Uses of clays in waste managements: toxic and non-toxic. *The Science of*
1028 *Clays* 309–325 (2013).
- 1029 169. Sellin, P. & Leupin, O. X. The use of clay as an engineered barrier in radioactive-waste
1030 management—a review. *Clays and Clay Minerals* **61**, 477–498 (2013).
- 1031 170. Wypych, F., Bergaya, F. & Schoonheydt, R. A. From polymers to clay polymer
1032 nanocomposites. *Developments in clay science* **9**, 331–359 (2018).
- 1033 171. Bergaya, F. & Lagaly, G. Chapter 10.0 - Introduction on Modified Clays and Clay Minerals.
1034 *Handbook of Clay Science* **5**, 383 – (2013).
- 1035 172. Vicente, M. A., Gil, A. & Bergaya, F. Chapter 10.5 - Pillared Clays and Clay Minerals.
1036 *Handbook of Clay Science* **5**, 523–557 (2013).
- 1037 173. Dutta, D. K. Clay mineral catalysts. *Developments in Clay Science* **9**, 289–329 (2018).
- 1038 174. Bhowmick, S. *et al.* Montmorillonite-supported nanoscale zero-valent iron for removal
1039 of arsenic from aqueous solution: Kinetics and mechanism. *Chemical Engineering*
1040 *Journal* **243**, 14–23 (2014).
- 1041 175. Han, H. *et al.* A critical review of clay-based composites with enhanced adsorption
1042 performance for metal and organic pollutants. *Journal of hazardous materials* **369**, 780–
1043 796 (2019).
- 1044 176. Yadav, V. B., Gadi, R. & Kalra, S. Clay based nanocomposites for removal of heavy metals
1045 from water: A review. **232**, 803–817 (2019).
- 1046 177. Zhang, T. *et al.* Removal of heavy metals and dyes by clay-based adsorbents: From
1047 natural clays to 1D and 2D nano-composites. *Chemical Engineering Journal* 127574
1048 (2020).

- 1049 178. Buruga, K. *et al.* A review on functional polymer-clay based nanocomposite membranes
1050 for treatment of water. *Journal of hazardous materials* **379**, 120584 (2019).
- 1051 179. Jlassi, K., Chehimi, M. M. & Thomas, S. *Clay-polymer nanocomposites*. (Elsevier: 2017).
- 1052 180. Payne, T. E. *et al.* Guidelines for thermodynamic sorption modelling in the context of
1053 radioactive waste disposal. *Environmental modelling & software* **42**, 143–156 (2013).
- 1054 181. Caporale, A. G. & Violante, A. Chemical processes affecting the mobility of heavy metals
1055 and metalloids in soil environments. *Current Pollution Reports* **2**, 15–27 (2016).
- 1056 182. Manceau, A. *et al.* Quantitative Zn speciation in smelter-contaminated soils by EXAFS
1057 spectroscopy. *American Journal of Science* **300**, 289–343 (2000).
- 1058 183. Appelo, C. A. J., Vinsot, A., Mettler, S. & Wechner, S. Obtaining the porewater
1059 composition of a clay rock by modeling the in- and out-diffusion of anions and cations
1060 from an in-situ experiment. *Journal of Contaminant Hydrology* **101**, 67–76 (2008).
- 1061 184. Appelo, C. A. J. & Wersin, P. Multicomponent diffusion modeling in clay systems with
1062 application to the diffusion of tritium, iodide, and sodium in Opalinus clay.
1063 *Environmental Science & Technology* **41**, 5002–5007 (2007).
- 1064 185. Soler, J. M., Steefel, C. I., Gimmi, T., Leupin, O. X. & Cloet, V. Modeling the ionic strength
1065 effect on diffusion in clay. The DR-A experiment at Mont Terri. *ACS Earth and Space*
1066 *Chemistry* **3**, 442–451 (2019).
- 1067 186. Gimmi, T. & Kosakowski, G. How mobile are sorbed cations in clays and clay rocks?
1068 *Environmental Science & Technology* **45**, 1443–1449 (2011).
- 1069 187. Glaus, M. *et al.* Cation diffusion in the electrical double layer enhances the mass transfer
1070 rates for Sr²⁺, Co²⁺ and Zn²⁺ in compacted illite. *Geochimica et Cosmochimica Acta*
1071 **165**, 376–388 (2015).
- 1072 188. Glaus, M., Frick, S. & Van Loon, L. A coherent approach for cation surface diffusion in
1073 clay minerals and cation sorption models: Diffusion of Cs⁺ and Eu³⁺ in compacted illite
1074 as case examples. *Geochimica et Cosmochimica Acta* **274**, 79–96 (2020).
- 1075 189. Borst, A. M. *et al.* Adsorption of rare earth elements in regolith-hosted clay deposits.
1076 *Nature communications* **11**, 1–15 (2020).
- 1077 190. Chi, R., Tian, J. & others *Weathered crust elution-deposited rare earth ores*. (Nova
1078 Science Publishers: 2008).
- 1079 191. Li, Y. H. M., Zhao, W. W. & Zhou, M.-F. Nature of parent rocks, mineralization styles and
1080 ore genesis of regolith-hosted REE deposits in South China: an integrated genetic model.
1081 *Journal of Asian Earth Sciences* **148**, 65–95 (2017).
- 1082 192. Moldoveanu, G. & Papangelakis, V. An overview of rare-earth recovery by ion-exchange
1083 leaching from ion-adsorption clays of various origins. *Mineralogical Magazine* **80**, 63–
1084 76 (2016).
- 1085 193. Sanematsu, K., Kon, Y., Imai, A., Watanabe, K. & Watanabe, Y. Geochemical and
1086 mineralogical characteristics of ion-adsorption type REE mineralization in Phuket,
1087 Thailand. **48**, 437–451 (2013).
- 1088 194. Li, M. Y. H., Zhou, M.-F. & Williams-Jones, A. E. The genesis of regolith-hosted heavy rare
1089 earth element deposits: Insights from the world-class Zudong deposit in Jiangxi
1090 Province, South China. *Economic Geology* **114**, 541–568 (2019).
- 1091 195. Goodenough, K. M., Wall, F. & Merriman, D. The rare earth elements: demand, global
1092 resources, and challenges for resourcing future generations. *Natural Resources*
1093 *Research* **27**, 201–216 (2018).
- 1094 196. Jordens, A., Cheng, Y. P. & Waters, K. E. A review of the beneficiation of rare earth
1095 element bearing minerals. *Minerals Engineering* **41**, 97–114 (2013).

- 1096 197. Berger, A., Janots, E., Gnos, E., Frei, R. & Bernier, F. Rare earth element mineralogy and
1097 geochemistry in a laterite profile from Madagascar. *Applied geochemistry* **41**, 218–228
1098 (2014).
- 1099 198. Bern, C. R., Yesavage, T. & Foley, N. K. Ion-adsorption REEs in regolith of the Liberty Hill
1100 pluton, South Carolina, USA: an effect of hydrothermal alteration. *Journal of*
1101 *Geochemical Exploration* **172**, 29–40 (2017).
- 1102 199. Sanematsu, K. & Watanabe, Y. Characteristics and Genesis of Ion Adsorption-Type Rare
1103 Earth Element Deposits. *Rare Earth and Critical Elements in Ore Deposits* (2016).
- 1104 200. Yamaguchi, A., Honda, T., Tanaka, M., Tanaka, K. & Takahashi, Y. Discovery of ion-
1105 adsorption type deposits of rare earth elements (REE) in Southwest Japan with
1106 speciation of REE by extended X-ray absorption fine structure spectroscopy.
1107 *Geochemical Journal* **52**, 415–425 (2018).
- 1108 201. Braun, J.-J. *et al.* Cerium anomalies in lateritic profiles. *Geochimica et Cosmochimica*
1109 *Acta* **54**, 781–795 (1990).
- 1110 202. Takahashi, Y., Shimizu, H., Usui, A., Kagi, H. & Nomura, M. Direct observation of
1111 tetravalent cerium in ferromanganese nodules and crusts by X-ray-absorption near-
1112 edge structure (XANES). *Geochimica et Cosmochimica Acta* **64**, 2929–2935 (2000).
- 1113 203. Moldoveanu, G. A. & Papangelakis, V. G. Recovery of rare earth elements adsorbed on
1114 clay minerals: I. Desorption mechanism. *Hydrometallurgy* **117**, 71–78 (2012).
- 1115 204. Jones, D. J., Rozière, J., Olivera-Pastor, P., Rodríguez-Castellón, E. & Jimenez-López, A.
1116 Local environment of intercalated lanthanide ions in vermiculite. *Journal of the*
1117 *Chemical Society, Faraday Transactions* **87**, 3077–3081 (1991).
- 1118 205. Takahashi, Y., Kimura, T., Kato, Y., Minai, Y. & Tominaga, T. Characterization of Eu (III)
1119 species sorbed on silica and montmorillonite by laser-induced fluorescence
1120 spectroscopy. *Radiochimica Acta* **82**, 227–232 (1998).
- 1121 206. Stumpf, T., Bauer, A., Coppin, F., Fanghänel, T. & Kim, J.-I. Inner-sphere, outer-sphere
1122 and ternary surface complexes: a TRLFS study of the sorption process of Eu (III) onto
1123 smectite and kaolinite. *Radiochimica Acta* **90**, 345–349 (2002).
- 1124 207. Mukai, H., Kon, Y., Sanematsu, K., Takahashi, Y. & Ito, M. Microscopic analyses of
1125 weathered granite in ion-adsorption rare earth deposit of Jianxi Province, China.
1126 *Scientific reports* **10**, 1–11 (2020).
- 1127 208. Velde, B. B. & Meunier, A. *The origin of clay minerals in soils and weathered rocks.*
1128 (Springer Science & Business Media: 2008).
- 1129 209. Nagasawa, M., Qin, H.-B., Yamaguchi, A. & Takahashi, Y. Local Structure of Rare Earth
1130 Elements (REE) in Marine Ferromanganese Oxides by Extended X-ray Absorption Fine
1131 Structure and Its Comparison with REE in Ion-adsorption Type Deposits. *Chemistry*
1132 *Letters* **49**, 909–911 (2020).
- 1133 210. Ohta, A., Kagi, H., Tsuno, H., Nomura, M. & Kawabe, I. Influence of multi-electron
1134 excitation on EXAFS spectroscopy of trivalent rare-earth ions and elucidation of change
1135 in hydration number through the series. *American Mineralogist* **93**, 1384–1392 (2008).
- 1136 211. Stumpf, S. *et al.* Sorption of Am (III) onto 6-line-ferrihydrite and its alteration products:
1137 Investigations by EXAFS. *Environmental science & technology* **40**, 3522–3528 (2006).
- 1138 212. Ohta, A., Kagi, H., Nomura, M., Tsuno, H. & Kawabe, I. Coordination study of rare earth
1139 elements on Fe oxyhydroxide and Mn dioxides: Part II. Correspondence of structural
1140 change to irregular variations of partitioning coefficients and tetrad effect variations
1141 appearing in interatomic distances. *American Mineralogist* **94**, 476–486 (2009).

- 1142 213. Kashiwabara, T. *et al.* Synchrotron X-ray spectroscopic perspective on the formation
1143 mechanism of REY-rich muds in the Pacific Ocean. *Geochimica et Cosmochimica Acta*
1144 **240**, 274–292 (2018).
- 1145 214. Butt, C. R. & Cluzel, D. Nickel laterite ore deposits: weathered serpentinites. *Elements*
1146 **9**, 123–128 (2013).
- 1147 215. Bergaya, F. & Lagaly, G. Chapter 1 - General Introduction: Clays, Clay Minerals, and Clay
1148 Science. *Handbook of Clay Science. Part A. Fundamentals* **5**, 1–19 (2013).
- 1149 216. Schoonheydt, R. A., Johnston, C. T. & Bergaya, F. Clay minerals and their surfaces.
1150 *Developments in Clay Science* **9**, 1–21 (2018).
- 1151 217. Hohenberg, P. & Kohn, W. Inhomogeneous electron gas. *Physical review* **136**, B864
1152 (1964).
- 1153 218. Kohn, W. & Sham, L. J. Self-consistent equations including exchange and correlation
1154 effects. *Physical review* **140**, A1133 (1965).
- 1155 219. Marx, D. & Hutter, J. *Ab initio molecular dynamics: basic theory and advanced methods*.
1156 (Cambridge University Press: 2009).
- 1157 220. Frenkel, D. & Smit, B. *Understanding molecular simulation: from algorithms to*
1158 *applications*. (Academic Press: 2002).
- 1159 221. Liu, X., Tournassat, C. & Steefel, C. I. Preface to multiscale simulation in geochemistry.
1160 **291**, 1–4 (2020).
- 1161 222. Sposito, G. *The surface chemistry of natural particles*. 242 (Oxford University Press: New
1162 York, 2004).
- 1163 223. Steefel, C. I. *et al.* Reactive transport codes for subsurface environmental simulation.
1164 *Computational Geosciences* **19**, 445–478 (2015).
- 1165 224. Steefel, C. I. Reactive transport at the crossroads. *Reviews in Mineralogy &*
1166 *Geochemistry* **85**, 1–26 (2019).

1167
1168

1169 **Acknowledgements**

1170 XL was supported by the National Natural Science Foundation of China (Nos. 42125202 and 41872041). CT, SG
1171 and AMF acknowledge funding from the EC Horizon 2020 project EURAD under Grant Agreement 847593 (WP
1172 FUTURE). CT research at LBNL was supported by the U.S. Department of Energy, Office of Science, Office of
1173 Basic Energy Sciences, Chemical Sciences, Geosciences, and Biosciences Division, through its Geoscience
1174 program at LBNL under Contract DE-AC02-05CH11231. CT acknowledges a grant overseen by the French
1175 National Research Agency (ANR) as part of the “Investissements d’Avenir” Programme LabEx VOLTAIRE, 10-
1176 LABX-0100 at ISTO. S.G. acknowledges partial funding by an in-house BRGM grant.

1177 **Author contributions**

1178 XL and CT were responsible for the design and compilation of the article. All authors contributed to the
1179 writing and editing.

1180 **Competing interests**

1181 The authors declare no competing interests.

1182

1183 **Peer review information**

1184 *Nature Reviews Earth & Environment* thanks J. Kubicki, B. Sarkar, and the other, anonymous, reviewer(s)
1185 for their contribution to the peer review of this work.

1186 **Publisher's note**

1187 Springer Nature remains neutral with regard to jurisdictional claims in published maps and institutional
1188 affiliations.

1189

1190 **Key points:**

1191 • Clay minerals have a diverse array of chemical structures and layer types that lead to a range
1192 of metal ion retention mechanisms in Earth's critical zone. The metal retention capabilities of
1193 clay minerals can concentrate rare earth elements (REEs) in ion adsorption type deposits and
1194 can also be exploited for metallic industrial waste disposal.

1195 • Basic metal ion-clay mineral interaction mechanisms include cation exchange, surface
1196 complexation, ligand exchange, structural incorporation, surface precipitation (with or
1197 without epitaxial growth of neoformed minerals), and precipitation induced by surface redox
1198 reactions.

1199 • Such diversity of retention mechanisms originates from the distinct structures and properties
1200 of basal and edge surfaces. Cation exchange on basal surfaces occurs mainly through
1201 electrostatics while other mechanisms occur through chemical bonding on edge surfaces.

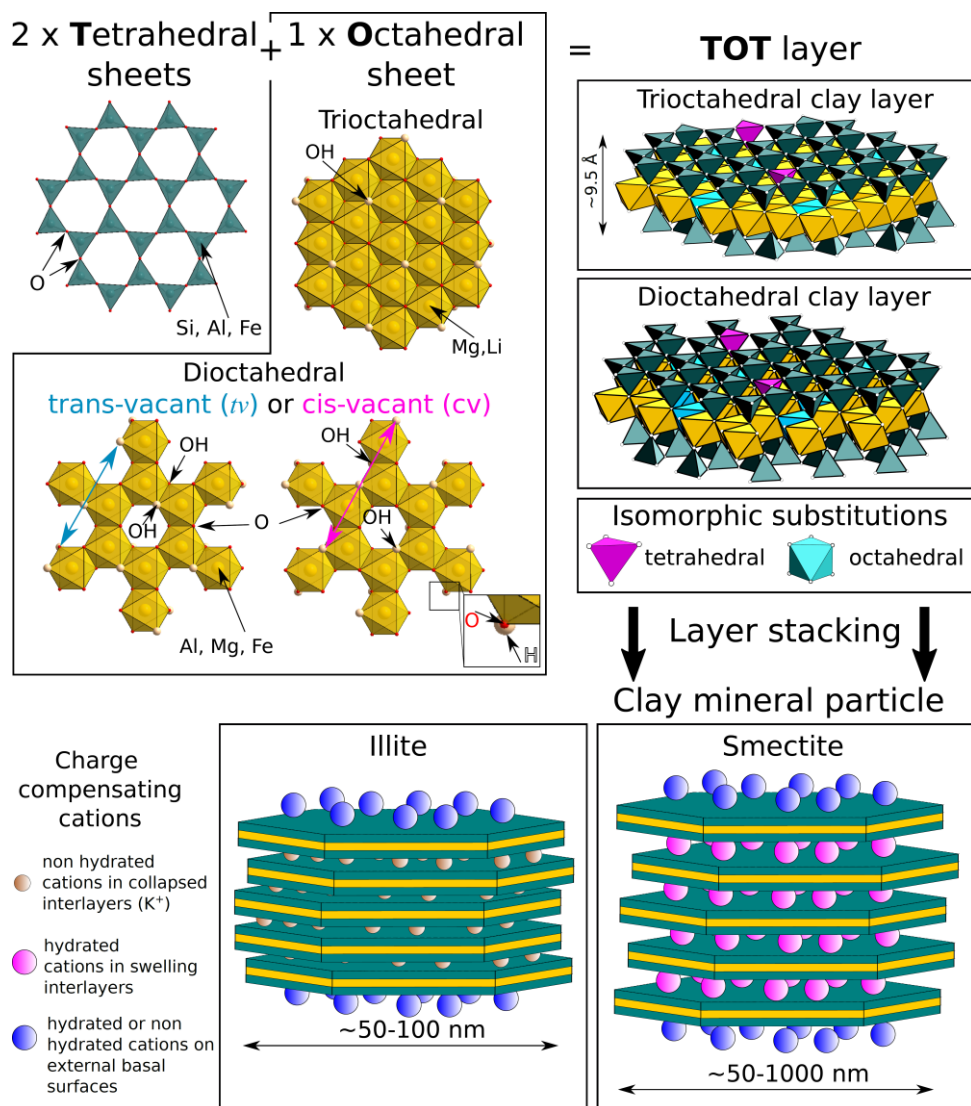
1202 • REEs in ion adsorption type deposits are mainly physically adsorbed on basal surfaces, which
1203 are responsible for the high REE extractability (> 50 %) through ion exchange.

1204 • Both cation exchange and surface complexation processes occur during the retardation of
1205 metallic pollution plumes in waste management applications (radioactive and conventional
1206 industrial wastes as well as landfill leachate).

1207 • Understanding and quantification of the multifaceted and multiscale nature of clay mineral-
1208 metal ion interactions necessitates the close combination of experimental and modelling
1209 techniques at the molecular-level.

1210

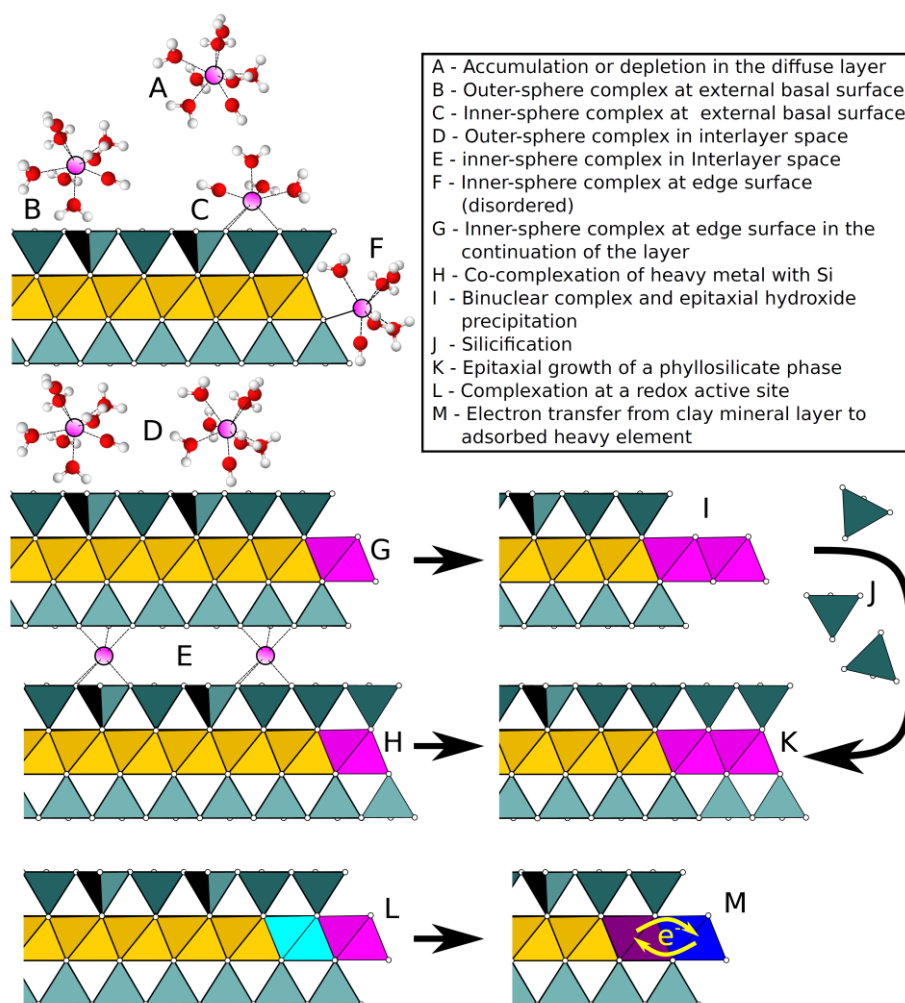
1211



1213

1214 **Figure 1. Clay mineral sheet, layer and particle structures.** Two tetrahedral sheets
 1215 sandwiching an octahedral sheet form a tetrahedral-octahedral-tetrahedral (TOT) layer. The
 1216 thickness of a TOT layer, ~9.5 Å, corresponds to the distance between two planes of apical
 1217 oxygen atoms, ~6.6 Å, plus the ionic radii of two oxygen atoms. Isomorphous substitutions
 1218 (where one structural cation is replaced for another of similar size, see magenta tetrahedral and
 1219 cyan octahedral) are responsible for a permanent negative structural layer charge that is
 1220 compensated by cations present in the interlayer spaces and on external surfaces of clay mineral
 1221 particles. In water-saturated conditions, charge compensating cations can be hydrated (red and
 1222 blue cations) or not (yellow cations), depending on the nature of the cation, the type of layer
 1223 isomorphous substitutions, the layer charge, and the type of neighbouring surfaces (interlayer
 1224 versus external). Layer structure and negative charge are responsible for the high metal cation
 1225 retention capability of clay minerals.

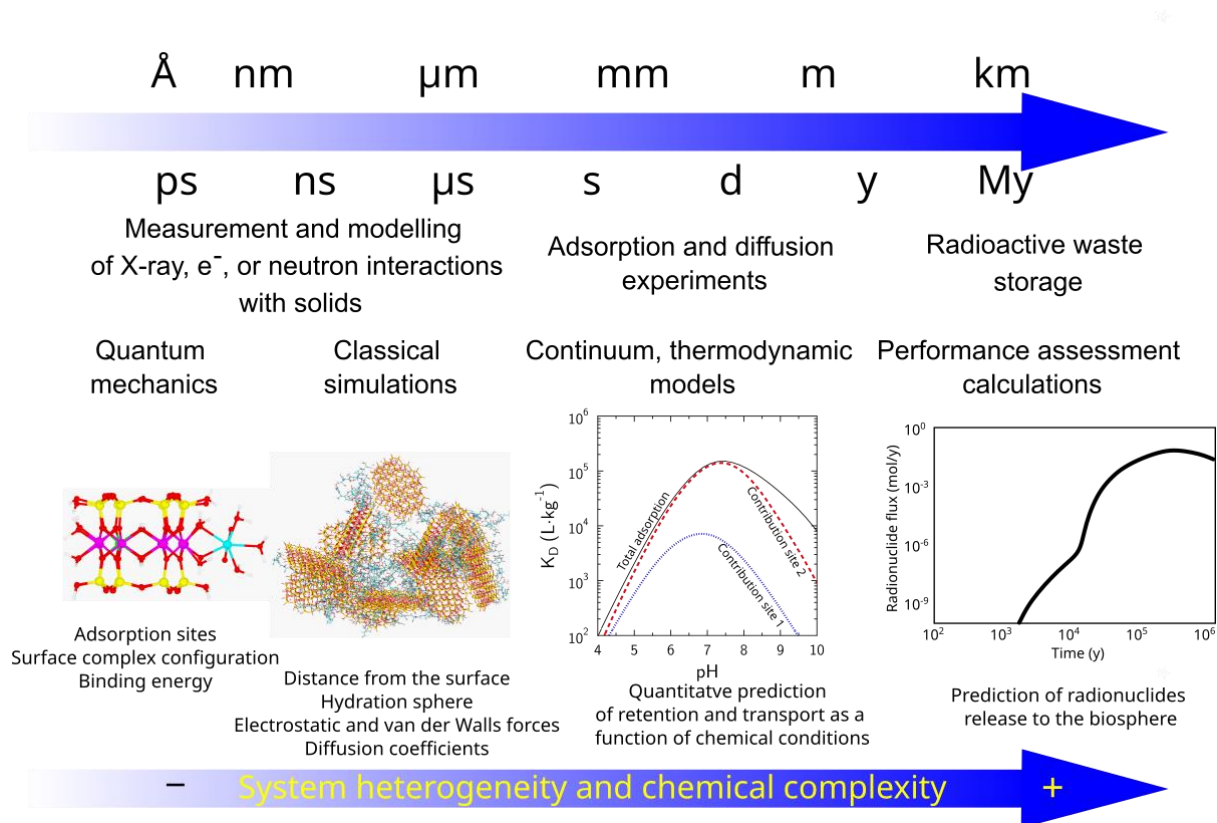
1226



1228

1229 **Figure 2. Interaction mechanisms of metal ions with clay minerals.** Clay layers are made of
 1230 octahedral (orange) and tetrahedral (blue) sheets, depicted along the stacking direction.
 1231 Adsorbed metal ions are shown in purple, and water molecules in red and white. a| Metal ions
 1232 (purple) in complexes with water molecules (red-white) can be adsorbed onto external basal
 1233 surfaces or accumulate in diffuse layers. The transitions from panels b to d highlight the
 1234 continuum from adsorption on edge surfaces to clay mineral nucleation and growth. b| outer-
 1235 sphere complexes can be adsorbed in the interlayer space. Inner-sphere complexes can attach
 1236 onto the edge of the octahedral layer, or c| in the interlayer space. If complexation of the edge
 1237 surface occurs at the same time as silicification, the clay mineral undergoes epitaxial growth.
 1238 d| A cation adsorbed by complexation at an active redox site on an edge surface can undergo
 1239 electron transfer with the clay mineral layer, which in turn changes the redox state of both the
 1240 octahedral sheet and adsorbed metal ions (blue-purple colour change). The duality of surface
 1241 types (basal vs. edge) and the redox reactivity of the inner atoms in the layer are responsible
 1242 for multiple modes of interactions with metal cations.

1243



1244

1245 **Figure 3. Upscaling of information in modeling of radionuclide storage.** a| Quantum
 1246 mechanical simulation of a metal ion complexed on clay mineral surface. b| Classical
 1247 simulation of metal ions at a clay mineral-aqueous solution interface. c| An example of a
 1248 surface complexation model for metal ion adsorption on clay mineral surfaces using a two-site
 1249 model. Information about binding energy and the nature of adsorption sites can be constrained
 1250 by molecular level studies. d| generic example of a simulation of radionuclide flux at the outlet
 1251 of a radioactive waste storage site over 1000-100,000 year time scales. Retention and diffusion
 1252 parameters used in these simulations are usually obtained in laboratory experiments that last
 1253 from days to years. Using these parameters to make upscaled predictions to million year time
 1254 scales must be justified by process understanding and quantification. Effective upscaling of
 1255 molecular-level information from measurements and simulations enables practical applications
 1256 in macroscopic studies.

1257

1258

1259

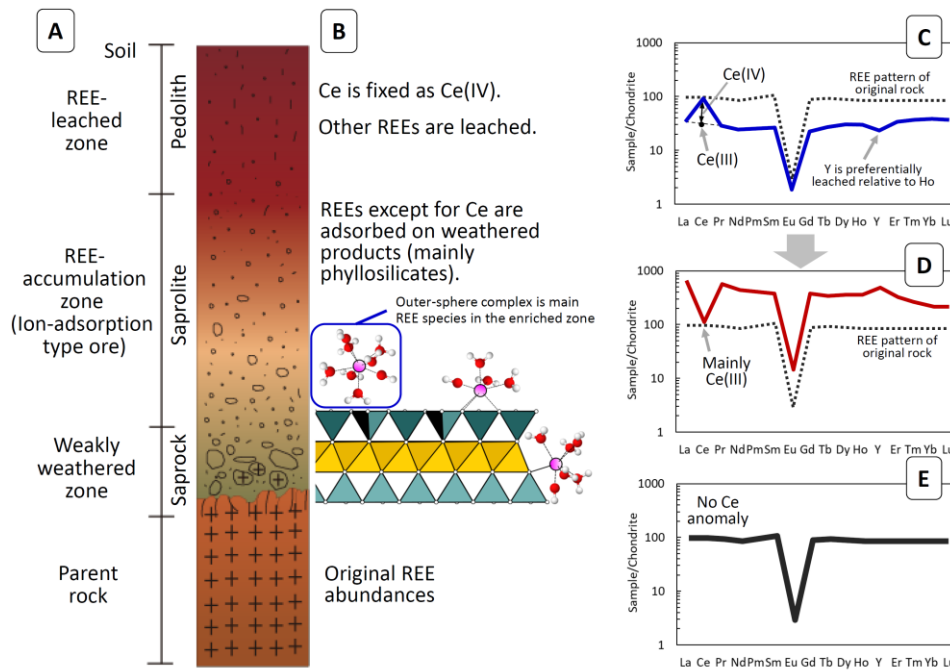
1260

1261

1262

1263

1264



1265

1266 **Figure 4. Ion-adsorption type rare earth element (REE) deposits. a** | Typical vertical profile
 1267 of weathered zone hosting ion-adsorption deposit (IAD). Granite is a typical parent rock for
 1268 IADs. **b** | Rare earth elements, excluding Ce, are leached from the top layer in the profile (the
 1269 pedolith). REE accumulation occurs in saprolite deposits, below the pedolith but above the
 1270 weathered parent rock. Adsorption of REEs in the accumulation zone mainly occurs as outer-
 1271 sphere complexes on external basal clay layers. **c** | the REE-leached zone is characterized by a
 1272 positive cerium (Ce) anomaly and relatively low REE abundances. Y is preferentially leached
 1273 relative to Ho. **d** | the REE-accumulation zone is characterized by a negative Ce anomaly and
 1274 enrichment of the other REEs. Y is enriched relative to Ho. **e** | the weakly weathered zone has
 1275 a similar REE pattern to the parent rock, but does not have the Ce anomaly. Adsorption on clay
 1276 minerals as outer-sphere complex is responsible for the enrichment and high extraction rate of
 1277 REEs in IAD.

1278

1279

1280

1281

1282

1283

1284

1285

1286 **Boxes**

1287 **Box 1. Clay mineral structures and surfaces**

1288 Clay minerals are phyllosilicates. They are made up of stacked layers consisting of an
1289 assemblage of sheets. Chemical composition, spatial arrangement of sheets, and layer stacking
1290 mode are the main criteria that identify clay mineral family members²¹⁵.

1291 Layers of dioctahedral smectite and illite, two groups of clay minerals of interest for their metal
1292 ions retention properties, are made of two tetrahedral sheets sandwiching an octahedral sheet,
1293 forming so-called 2:1 layers (Figure 1).

1294 Tetrahedral and octahedral sheets of smectite and illite contain mostly Si and Al (or Fe) atoms.
1295 A range of other minor elements are incorporated through isomorphic substitutions, which
1296 create a local charge imbalance if the substituted element does not bear the same formal charge
1297 as the incorporated element (for example, Mg^{2+} for Al^{3+}). This local charge is not compensated
1298 for in the layer structure, which creates a permanent negative structural charge in the clay layer.
1299 This negative charge is compensated by the positive charge of cations in the interlayer space
1300 and on external surfaces.

1301 Interlayer spaces can be hydrated and accessible to aqueous species as in the case of smectite,
1302 or collapsed and mostly inaccessible to water and aqueous species as in the case of illite, in
1303 which adjacent tetrahedral sheets are bonded by non-hydrated K^+ ions (Figure 1). Na^+ , K^+ ,
1304 Ca^{2+} , Mg^{2+} are the most common charge compensating cations, but they can be exchanged
1305 easily on external and hydrated interlayer surfaces by other metal cations⁶⁸. Differences in
1306 hydration properties of interlayer cations results in the common phenomenon of clay mineral
1307 swelling, which corresponds to changes of interlayer spacing as a function of the nature of
1308 interlayer cations and water chemical potential²¹⁶.

1309 Crystal faces of clay minerals can be grouped into basal and edge surfaces, which are parallel
1310 and perpendicular to the basal plane respectively⁶⁸. Smectite and illite layers thickness is
1311 approximately 1 nm, while their lateral dimensions range from 50 nm to 1 μm (Figure 1). These
1312 dimensions result in very large specific surface areas, up to 800 $m^2 g^{-1}$ for smectites. The vast
1313 majority of the surface area is born by the basal surfaces, while edge surface area account for
1314 only 5 to 30 $m^2 g^{-1}$.

1315 Atoms present at basal surfaces are fully coordinated and form a siloxane terminated surface,
1316 while oxygen atoms present at edge surfaces have fewer metal neighbours than in bulk (Figure
1317 1). Edge surfaces are covered by chemically adsorbed water, forming amphoteric charged
1318 surface hydroxyl groups ($>OH$ groups, where the $>$ sign is indicative of a surface coordination),
1319 having contrasted acidity constants (pK_a) as a function of coordination, surface crystallographic
1320 orientation and nature of the central metal bonded to the $>OH$ group⁸⁸. Consequently, edge
1321 surface chemical properties are strongly pH-dependent, by contrast, basal surface properties
1322 are little or not.

1323

1324 **Box 2. Quantification of metal ion immobilisation**

1325 Macroscopic quantification of metal ion retention on a given mass of clay minerals (m_{clay} in
 1326 kg) can be obtained from experimental adsorption isotherms (see figure). The concentration of
 1327 an adsorbed element (C_{ads} in $\text{mol kg}^{-1}_{clay}$) can be quantified by the difference between a total
 1328 concentration added in the system (C_{tot} in mol L^{-1}) and an aqueous concentration measured at
 1329 steady-state, which is assumed to be representative of thermodynamic equilibrium (C_{eq} in mol
 1330 L^{-1}).

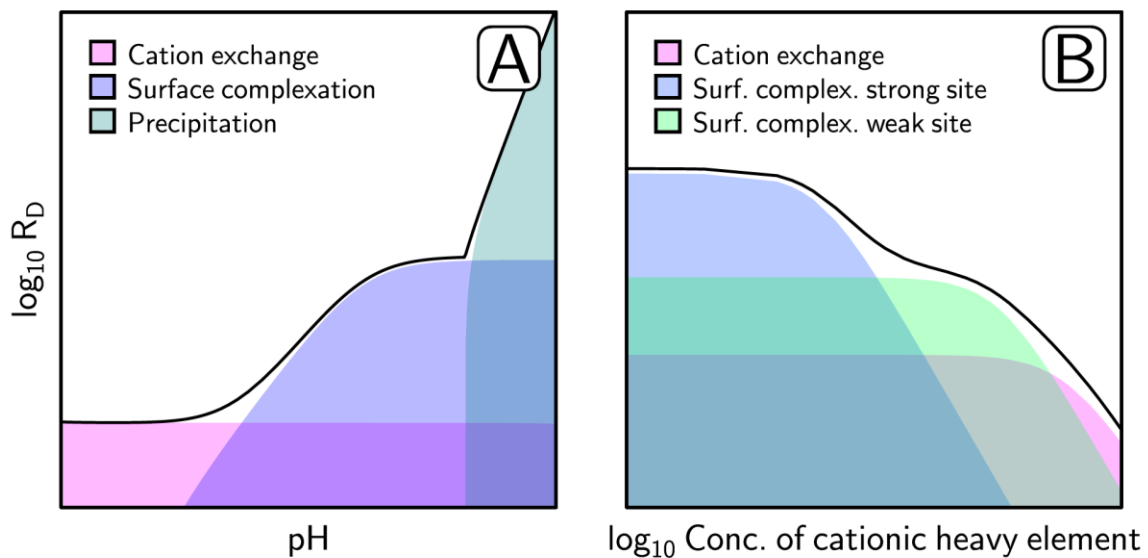
1331
 1332 Retention is usually quantified as a percentage of total added concentration, or as a distribution
 1333 coefficient R_D , or K_D (in L kg^{-1}), which quantify the partitioning of the metal ions between the
 1334 solution and the surface:

$$C_{ads} = \frac{C_{tot} - C_{eq}}{m_{clay}} V_{sol} \quad 1$$

$$R_D \text{ or } K_D = \frac{C_{ads}}{C_{eq}} \quad 2$$

1335 where V_{sol} is the volume of solution (in L).

1336 The R_D value does not give any insight into the physical and chemical processes responsible
 1337 for the observed retention (such as adsorption, incorporation, and precipitation). However, in
 1338 a first approach, the shape of the adsorption isotherms plotted as a function of pH and metal
 1339 ion concentration (see figure), allows the difference between major adsorption sites and other
 1340 retention mechanisms to be determined.



1341

1342 The figure shows: **a|** retention processes shown as a function of pH and constant metal cations
 1343 concentration, and **b|** as a function of metal cations concentration and fixed pH. Superposition
 1344 of coloured areas is indicative of a mixed contribution of several mechanisms to the overall
 1345 retention.

1346

1347

1348 **Box 3. Predictive approaches at different scales**

1349 **Quantum mechanics simulation**

1350 Density functional theory (DFT)^{217,218} has been the workhorse of quantum mechanics
1351 calculation. By transforming the 3N-dimensional Schrodinger equation to 3-dimensional
1352 Kohn-Sham equation, DFT makes it affordable to calculate energy and atomic forces of
1353 realistic systems. First principles molecular dynamics (FPMD)²¹⁹, a combination of DFT and
1354 molecular dynamics (MD), generates dynamical trajectories at limited temperatures and is thus
1355 able to explore the properties of aqueous and interfacial systems. FPMD can calculate free
1356 energy by integrating with enhanced sampling techniques (such as the method of constraint,
1357 metadynamics). However, the expensive computational costs badly limits the system size and
1358 time FPMD can access: for current supercomputing architecture the typical length and time
1359 scales are only ~10 angstroms and ~10 picoseconds.

1360 **Classical simulation**

1361 Classical simulation calculates energy and forces based on a force field that is a set of
1362 parameters describing atomic interactions²²⁰. Classical MD produces dynamical trajectories by
1363 using the forces calculated from a force field. The length and timescale of classical simulation
1364 can reach second and micrometer.

1365 **Multiscale simulation**

1366 Classical mechanical simulation and thermodynamic models are necessary to build direct link
1367 to macroscopic experiments. These models are usually based on a set of empirical/fitted
1368 parameters. Multiscale simulation plays the role of a bridge by translating the information
1369 generated by quantum mechanics into parameters of upscaling modelling, thus overcoming the
1370 temporal and spatial limits of quantum mechanics modelling, such as it provides constraints
1371 for geochemical modeling and the force field used in classical simulation²²¹.

1372 **Geochemical thermodynamic modeling**

1373 Surface complexation and cation exchange models apply mass balance, surface charge balance
1374 and thermodynamic chemical equilibrium concepts to predict, quantitatively, the partitioning
1375 of chemical species between an aqueous solution and mineral surfaces²²². Surface
1376 complexation and cation exchange models can be coupled to fluid transport models at large
1377 scale (aquifers, rivers, water catchment) to build defensible predictions in the environmental
1378 sciences^{223,224}. Since the ~2000s, model parameters have been obtained from fitting
1379 macroscopic adsorption, while microscopic and spectroscopic observations helped
1380 constraining the main mechanisms responsible for the observed metal ions retention. Since the
1381 ~2010s, advances in molecular level modelling and multiscale simulations provide new

1382 possibilities to reduce the number of empirical fitting parameters in surface complexation and
1383 cation exchange models.

1384 **Glossary terms:**

1385 **Metal ions:** metal cation (M) in aqueous solution with the chemical formula $[M(H_2O)_n]^{z+}$,
1386 metal ions include rare earth elements (REEs), actinides, transition metals, and alkaline and
1387 alkaline-earth metals.

1388 **Clay mineral:** signifies a class of hydrated phyllosilicates making up the fine-grained fraction
1389 of rocks, sediments, and soils, which this Review is focused on.

1390 **Clay-rich materials** refers to materials containing clay minerals, such as sediments, soils and
1391 weathered rocks, and with physical and chemical properties dominated by their clay mineral
1392 fraction.

1393 **Earth's Critical zone:** The oxygenated and hydrated layer at Earth's surface and shallow
1394 subsurface, spanning from the tops of tree canopies to the bottom of groundwater.

1395 **Complex:** a compound consisting of a central atom or ion that is bonded to other atoms or ions,
1396 which are called ligands.

1397 **Ligand exchange:** A type of reaction in which a ligand of a complex is replaced by a different
1398 ligand.

1399 **Tetrahedral sheet:** A 2-dimensional sheet formed by tetrahedral units, each consisting of a
1400 metal cation coordinated by four oxygen atoms and linked to three neighbouring tetrahedra by
1401 shared oxygen.

1402 **Octahedral sheet:** A 2-dimensional sheet formed by octahedral units, each consisting of a
1403 metal cation coordinated by six oxygen atoms, linked to six neighbouring octahedra by shared
1404 edges.

1405 **Diocahedral:** A common type of octahedral sheet where most of the metal cations are of +3
1406 valence, two-thirds of the octahedra are occupied while the other third is vacant.

1407 **2:1-type clay mineral:** clay mineral which has a structural layer made of one octahedral sheet
1408 sandwiched by two tetrahedral sheets.

1409 **Smectite:** A group of 2:1-type clay minerals with expandable interlayer space

1410 **Illite:** A group of 2:1-type clay minerals with non-expandable interlayer space.

1411 **Inner-sphere complex:** where the cation is adsorbed on a clay layer with direct chemical
1412 contact to the mineral layer surface.

1413 **Outer-sphere complex:** where the cation is adsorbed on a clay layer surface, but is separated
1414 by one or more water molecules.

1415 **Epitaxial nucleation:** formation of a crystalline nucleus on a substrate, where the new
1416 crystalline layers form with one or more well-defined orientations fixed by that of the substrate
1417 lattice.

1418 **Neutron diffraction:** an experimental technique used to probe the crystallographic properties
1419 of materials, including the position of hydrogen atoms, notably by taking advantage of the
1420 contrasting interactions of neutrons with hydrogen and deuterium.

1421 **Synchrotron X-ray reflectivity (XRR):** an experimental technique used to study the detailed
1422 surface properties of solids, based on the analysis of X-rays reflected by a surface.

1423 **X-ray absorption spectroscopy (XAS):** an experimental technique used to study oxidation
1424 state and local environment of an atom in a sample, based on analysis of variations in X-ray
1425 absorption over a range of photon energies.

1426

1427 **Website summary:**

1428 Clay minerals can retain metal ions, concentrate rare earth elements and be exploited for
1429 industrial waste disposal. This Review discusses the molecular-level mechanisms of metal ion
1430 retention in clay minerals and their importance for environmental and industrial applications.

1431

